

**Marginal reefs under stress: physiological limits render Galápagos corals
susceptible to ocean acidification and thermal stress**

Diane Thompson¹, Malcolm McCulloch², Julia E. Cole³, Emma V. Reed¹, Juan P. D'Olivo⁴,
Kelsey Dyez³, Marcus Lofverstrom¹, Janice Lough^{5,6}, Neal Cantin⁵, Alexander W. Tudhope⁷,
Anson H. Cheung⁸, Lael Vetter¹, R. Lawrence Edwards⁹

¹ University of Arizona, Department of Geosciences, Tucson, 85721, USA

² University of Western Australia, ARC Centre of Excellence for Coral Reefs Studies, Oceans
Graduate School and Oceans Institute, Crawley, 6009, Australia

³ University of Michigan, Earth and Environmental Sciences, Ann Arbor, 48109, USA

⁴ Freie Universität Berlin, Berlin, 12249, Germany

⁵ Australian Institute of Marine Science, PMB 3, Townsville MC, Queensland 4810, Australia

⁶ ARC Centre of Excellence for Coral Reef Studies, James Cook University, Townsville, Queensland
4811, Australia

⁷ University of Edinburgh, School of Geosciences, Edinburgh EH9 3JW, UK

⁸ Department of Earth, Environmental, and Planetary Sciences, Brown University, Providence, RI
02912

⁹ Department of Earth Sciences, University of Minnesota, Minneapolis, MN

1 **Marginal reefs under stress: physiological limits render**
2 **Galápagos corals susceptible to ocean acidification and thermal**
3 **stress**

4 **Short title: Physiological limits to corals' buffering capacity**

5 **Diane Thompson,^{1*} Malcolm McCulloch,² Julia E. Cole,³ Emma V. Reed,¹**
6 **Juan P. D'Olivo,⁴ Kelsey Dyez,³ Marcus Lofverstrom,¹ Janice Lough,^{5,6} Neal Cantin,⁵**
7 **Alexander W. Tudhope,⁷ Anson H. Cheung,⁸ Lael Vetter,¹ R. Lawrence Edwards⁹**

8 ¹University of Arizona, Department of Geosciences, Tucson, 85721, USA

9 ²University of Western Australia, ARC Centre of Excellence for Coral Reefs Studies, Oceans Graduate School and Oceans
10 Institute, Crawley, 6009, Australia

11 ³University of Michigan, Earth and Environmental Sciences, Ann Arbor, 48109, USA

12 ⁴Freie Universität Berlin, Berlin, 12249, Germany

13 ⁵Australian Institute of Marine Science, PMB 3, Townsville MC, Queensland 4810, Australia

14 ⁶ARC Centre of Excellence for Coral Reef Studies, James Cook University, Townsville, Queensland 4811, Australia

15 ⁷University of Edinburgh, School of Geosciences, Edinburgh EH9 3JW, U.K.

16 ⁸Department of Earth, Environmental, and Planetary Sciences, Brown University, Providence, RI 02912

17 ⁹Department of Earth Sciences, University of Minnesota, Minneapolis, MN

18 **Key Points:**

- 19 • Carbonate saturation of the internal growth medium is reduced in modern Galápagos *Porites*
20 corals, particularly following warm extremes.
21 • Corals display similar capacity to regulate their growth medium among sites and time periods,
22 with limited adaptation to acidification.
23 • Taken together, these results suggest strict physiological limits to corals' ability to buffer against
24 changing ocean conditions.

Corresponding author: Diane M. Thompson, thomsod@arizona.edu

Abstract

Ocean acidification and thermal stress may undermine corals' ability to calcify and support diverse reef communities, particularly in marginal environments. Coral calcification depends on aragonite supersaturation ($\Omega \gg 1$) of the calcifying fluid (cf) from which the skeleton precipitates. Corals actively upregulate pH_{cf} relative to seawater to buffer against changes in temperature and dissolved inorganic carbon (DIC_{cf}), which together control Ω_{cf} . Here we assess the buffering capacity in modern and fossil corals from the Galápagos Islands that have been exposed to sub-optimal conditions, extreme thermal stress, and ocean acidification. We demonstrate a significant decline in pH_{cf} and Ω_{cf} since the pre-industrial era, trends which are exacerbated during extreme warm years. These results suggest that there are likely physiological limits to corals' pH buffering capacity, and that these constraints render marginal reefs particularly susceptible to ocean acidification.

Plain Language Summary

Reef-building corals regulate their internal environment to permit rapid growth, which is critical for creating the structure and function of coral reefs. However, we demonstrate that there are finite limits to the ability of corals to regulate their internal chemistry to optimize growth. This limitation will leave corals susceptible to ocean warming and acidification, particularly in sub-optimal environments. Galápagos corals already display signs of stress and an inability to maintain an optimal internal growth environment from the 18th century to today.

Introduction

The carbonate structures of coral reef ecosystems provide critical defenses against storm surge and sea-level rise, supporting billions of dollars of goods and services annually beyond their intrinsic value (Spalding et al., 2017) and highlighting the need to understand how changing ocean conditions impact coral calcification. Thermal stress and ocean acidification (OA) diminish coral calcification, as shown in both experimental systems and Free Ocean CO_2 Enrichment (FOCE) experiments on natural reefs (Gattuso et al., 2014). Analyses of coral density variations in cores of massive corals also reveal declining coral calcification through time (J. M. Lough, 2010). Collectively, these studies demonstrate spatially and temporally varying rates of calcification, with significant declines under recent extreme warming events and OA. Corals in the Galápagos Archipelago have been disproportionately impacted (P. W. Glynn et al., 2018), due to both extreme El Niño-related warming (P. W. Glynn et al., 1988; P. Glynn, 2001) and highly variable upwelling and pH/saturation state (D. P. Manzello et al., 2008; D. P. Manzello, 2010). These "marginal" reefs exhibit low species diversity and structural complexity (Darwin & Bonney, 1889; Cortés, 1997; P. Glynn, 2001; D. P. Manzello et al., 2008; P. W. Glynn et al., 2017), and have experienced acidification at rates of around -0.0026 (pH units, total scale) yr^{-1} over the last 1.5 decades (1997-2011, Sutton et al., 2014). Differential recovery rates along spatial pH gradients (D. P. Manzello et al., 2014) further demonstrate the importance of carbonate chemistry and calcification processes to reef health in this region. As CO_2 levels rise, changing patterns of OA and warming will increase the pressure on eastern equatorial Pacific and other marginal reef environments.

A critical question remains, however: do corals have the adaptive capacity to maintain sustainable calcification in the face of increasingly stressful environmental conditions? Here, we leverage advances in biomineralization and boron isotope systematics to assess how changes in energy availability alter rates of calcification, the chemistry of the calcifying fluid, and the geochemistry of the carbonate skeleton (Table S1). We use this understanding of coral biomineralization to elucidate the sus-

68 ceptibility of coral calcification to OA and thermal stress, and to assess the adaptive capacity of Galá-
69 pagos (*Porites* sp.) corals to changing ocean conditions.

70 In reef-building corals, calcification varies in response to internal (physiological) and external
71 (environmental) factors, and maintenance of aragonite supersaturation in their calcifying fluid (Ω_{cf}
72 $\gg 1$) is the ultimate factor that permits supercalcification and buffers against changes in seawater chem-
73 istry (M. McCulloch et al., 2012; Thompson, 2021). This state is achieved via upregulation of DIC
74 and pH in response to changing environmental conditions. For example, during cooler seasons, corals
75 upregulate the pH of their calcifying fluid (pH_{cf}) in response to a drop in metabolic (i.e., from zoo-
76 anthellar photosynthesis and coral respiration) DIC, resulting from reduced temperature and light (e.g.,
77 J. D’Olivo & McCulloch, 2017; M. T. McCulloch et al., 2017; Ross et al., 2017, 2019). Cool temper-
78 atures also slow calcification kinetics and reduce the buffering capacity of the coral calcifying fluid (hereafter
79 "thermodynamic" factors, Guo, 2019; Georgiou et al., 2015). By upregulating pH_{cf} , corals maintain
80 a stable aragonite saturation state, shifting the carbonate reactions to favor carbonate ion during the
81 winter months and preserving their ability to calcify despite large seasonal changes in DIC availabil-
82 ity and temperature (as reviewed by Thompson, 2021). If these processes operate across species and
83 reef environments, corals may be able to withstand changes in seawater pH.

84 However, our understanding of coral biomineralization processes largely depends on studies of
85 modern massive corals from regions with relatively low interannual climate and geochemical variabil-
86 ity (Fig. 1a-b). Although a few studies have leveraged natural CO_2 seeps to study coral biomineral-
87 ization under extreme conditions (Wall et al., 2016, 2019), corals likely respond differently to sharp
88 spatial gradients compared to temporal variations. In many marginal reef environments, strong ocean-
89 ographic variability and low aragonite saturation states make reef-building corals particularly suscep-
90 tible to changing ocean conditions. Further, such marginal reefs provide a potential analogue of fu-
91 ture reef patterns, as OA broadens the coverage of sub-optimal to marginal conditions.

92 Here, we capitalize on the large natural gradients across the Pacific in SST variability (Fig. 1a)
93 and aragonite saturation state (Fig. 1b) to understand the range of coral responses to ongoing warm-
94 ing and acidification. We apply a multi-proxy, multi-site synthesis of coral geochemistry, backed by
95 a novel Earth system modelling framework, to reconstruct and contextualize the impact of environ-
96 mental stresses on calcification and resiliency in Galápagos corals. We leverage geochemical tracers
97 of coral biomineralization (Table S-1)—skeletal B/Ca ($[\text{CO}_3^-]$), $\delta^{11}\text{B}$ (pH_{cf}), and U/Ca ($[\text{CO}_3^-]$)—that
98 constrain the calcifying fluid chemistry, including the aragonite saturation that governs calcification
99 rate (DeCarlo et al., 2018, 2015). We combine these with paleo-environmental tracers that primar-
100 ily reflect factors external to the coral calcification environment (Table S-1): Sr/Ca (Beck et al., 1992;
101 Corrège et al., 2000), Li/Mg (Hathorne, Felis, et al., 2013; Montagna et al., 2014), and $\delta^{18}\text{O}$ (Weber
102 & Woodhead, 1972; McConnaughey, 1989) (all primarily controlled by SST); Ba/Ca (upwelling, Lea
103 et al., 1989; G. T. Shen et al., 1992); and $\delta^{13}\text{C}$ (upwelling, metabolic carbon / photosynthesis, res-
104 piration, and reproduction, G. T. Shen et al., 1992). These new recent (1976-2010) and fossil (1729-
105 1733) Galápagos records (Wolf Island, $1^\circ 23.15'\text{N}$, $91^\circ 49.90'\text{W}$) significantly extend the multi-tracer
106 data coverage prior to the industrial era, which allows us to assess the capacity of corals to buffer against
107 changing environmental conditions. We compare our new Galápagos results with published data from
108 the Great Barrier Reef (M. T. McCulloch et al., 2017) to contextualize results from the marginal Galá-
109 pagos reef environment—a comparatively cold, low-saturation, and highly variable environment. Fi-
110 nally, we establish a comprehensive spatiotemporal framework for these results using simulations of
111 ocean biogeochemistry that extend from pre-industrial to modern (Fig. 1c), permitting the first cross-
112 Pacific, multi-century synthesis of corals’ ability to buffer calcifying fluid chemistry in response to chang-
113 ing ocean conditions, including acidification, warming, and (internal and forced) climate variability.



Figure 1. Map of study sites across tropical Pacific Ocean: (a) Interannual variability in sea-surface temperature (SST), calculated from standard deviation of CESM1 LME SST (see Fig. S2 for validation against IGOSS SSTs, Reynolds et al., 2002); (b) aragonite saturation state Ω_{sw} at 0m, calculated using CO2SYS (Lewis et al., 1998) from CESM1 LME temperature, salinity, pH_{sw} , and dissolved inorganic carbon (DIC) over the climatological period (1970-2005); and (c) difference in CESM1 LME Ω_{sw} between the modern and 18th century periods studied here. Simulated values for the Great Barrier Reef (Davies Reef) and Galápagos (Wolf Island) study sites are indicated by filled circles; validation of CESM1 against observational values can be found in Table S3.

114 Data and Methods

115 Coral Core Collection

116 We collected cores from modern (living) and underwater sub-fossil (i.e., deceased upon collec-
 117 tion; hereafter “fossil”) *Porites lobata* colonies in Shark Bay, along the northeastern shore of Wolf Is-
 118 land, Galápagos (1°23.15'N, 91°49.90'W) in May-June 2010. Here, we analyze four cores from three
 119 colonies (two modern, and one fossil): (1) GW10-3 (modern), collected from 10m depth; (2) GW10-
 120 10 (modern), collected from 12m depth; and (3) GW10-4 and (4) GW10-5 collected from the same
 121 fossil colony at 13m depth. We compare these geochemical records from Wolf to published data from
 122 Davies Reef, Great Barrier Reef (cores 13-2 and 13-3, M. T. McCulloch et al., 2017)).

123 Sub-sampling & Age Determination

124 All cores were milled for geochemical analysis at continuous 2 millimeter increments in 5mm-
 125 wide transects along the maximum growth axis; based on average modern extension rates (GW10-3
 126 = 12.4 mm/year, GW10-10 = 20.3 mm/year), this sampling increment resolves sub-seasonal (bimonthly
 127 or better) variability of coral skeletal geochemistry and inferred environmental parameters. This res-
 128 olution was selected based on the time- and sample-intensive nature of the ion exchange chromatog-
 129 raphy required for boron isotopic analysis; this work significantly extends the network of long, high-
 130 resolution, multi-proxy data. Modern corals were re-sampled adjacent to the original sampling tran-
 131 sects (Jimenez et al., 2018) across intervals of known climatic extremes (e.g., large eastern Pacific El
 132 Niño events) and phases of Pacific decadal variability, while fossil cores were sampled prior to and fol-
 133 lowing the depths sampled for U/Th age dating (to maximize precision of replicating and splicing these
 134 floating chronologies).

135 Pre-industrial Wolf fossil cores (WLF10-04 and WLF10-5) were U/Th dated at the University
 136 of Minnesota following the procedures of (Cheng et al., 2013; Edwards et al., 1987; C.-C. Shen et al.,
 137 2002). Wolf10-04 and WLF10-05 sample ages were 1732 ± 7 and 1738 ± 5 C.E., respectively (see Reed
 138 et al., 2021, for full U/Th results). These floating chronologies were tied to the complete Sr/Ca record
 139 from WLF10-4 (Reed et al., 2021) to optimize correlation among the series within the uncertainty of
 140 the U/Th dates. However, all Wolf fossil coral series are floating chronologies (i.e., they are not tied
 141 to overlapping modern records); thus, we estimate an absolute age error as $\pm 5-7$ years (based on the
 142 precision of the U/Th dates).

143 Age-depth models for all cores were developed using linear interpolation in MATLAB between
 144 seasonal Sr/Ca-SST tie points. Due to high interannual variability in the timing of the cool season
 145 minima the age model relies only on warm-season tie points. Sr/Ca minima were tied to March SST
 146 maxima; tie points for modern Wolf cores (WLF10-3 and WLF10-10) are identical to those published
 147 in Jimenez et al. (2018). Data were linearly interpolated to obtain monthly records for time-series anal-
 148 ysis. Although this approach may introduce sub-annual chronological errors, regressions among geo-
 149 chemical proxies that form the core of this study were performed on the raw data (prior to age mod-
 150 eling) and are not influenced by chronological errors or interpolation. Finally, we used Sr/Ca-SST re-
 151 constructions from GW10-3 (2010-1987; 1983-1940) and GW10-10 (2010-1985; 1982-1975) published
 152 by Jimenez et al. (2018) for comparison.

153 Trace Elemental Geochemistry

154 All trace elemental analyses were performed on a Quadrupole-ICP-MS (X-series II Q-ICP-MS,
 155 Thermo Fisher Scientific) at the University of Western Australia. First, sub-samples of 10 ± 0.2 mg

156 of coral powder were weighed, dissolved in 500 μL of 0.51N HNO_3 , agitated, and centrifuged for 1 minute
 157 at 3500rpm. A 38 μL aliquot of dissolved powder was diluted in 3 mL of 2% HNO_3 (100 ppm Ca) for
 158 trace elemental analysis; the remaining 400 μL of the dissolved powder was used for boron isotope anal-
 159 ysis (see below). Analysis of ^7Li , ^{25}Mg , and ^{11}B by Q-ICP-MS was performed on the 100 ppm Ca di-
 160 lution, while an additional 300 μL sub-aliquot of the 100 ppm Ca solution was diluted (to 10 ppm Ca)
 161 in 2.7 mL of a 2% HNO_3 spike solution (containing ~ 19 ppb ^{45}Sc , 19 ppb ^{89}Y , 0.19 ppb ^{141}Pr , and
 162 0.095 ppb ^{209}Bi) for analysis of ^{25}Mg , ^{43}Ca , ^{86}Sr , and ^{238}U . Although some recent work suggests that
 163 organic matter may bias TE/Ca values and increase analytical uncertainty (particularly for Li/Mg,
 164 Cuny-Guirriec et al., 2019), these issues were reported for green, organic-rich bands in the skeleton.
 165 As there were no green, organic-rich bands in our cores, we did not pre-treat the samples prior to geo-
 166 chemical analysis to avoid offsets and noise that can arise from oxidative cleaning under certain con-
 167 ditions (Holcomb et al., 2015; Sayani et al., 2021). Nevertheless, we note that the presence of organic
 168 matter in the samples could have caused small (1-4%) variations in trace elemental ratios and add noise
 169 to our data. Reproducibility for the JCP-1 interlaboratory standard (2σ relative standard deviation,
 170 RSD; $n = 19$) was $\pm 0.830\%$ for Mg/Ca, $\pm 0.636\%$ for Sr/Ca, $\pm 1.341\%$ for U/Ca, $\pm 3.649\%$ for Li/Mg
 171 ($N = 17$), and $\pm 3.651\%$ for B/Mg ($N = 17$). The long-term laboratory values for JCP-1 are well within
 172 the robust standard deviation of reported values from Hathorne, Gagnon, et al. (2013): Mg/Ca 4.211
 173 ± 0.024 mmol/mol ($n = 173$), Sr/Ca 8.848 ± 0.0194 mmol/mol ($n = 173$), Ba/Ca 7.297 ± 0.242 $\mu\text{mol/mol}$
 174 ($n = 159$), U/Ca 1.194 ± 0.0092 $\mu\text{mol/mol}$ ($n = 165$), Li/Mg 1.441 ± 0.0325 mmol/mol ($n = 144$),
 175 and B/Ca 458.956 ± 11.790 $\mu\text{mol/mol}$ ($n = 144$) (see also J. P. D’Olivo et al., 2018).

We used published TE/Ca-SST calibrations to reconstruct SST from the (local) Sr/Ca-SST (M. T. McCulloch et al., 2017; Jimenez et al., 2018) and Li/Mg-SST (Montagna et al., 2014) relationships. For Wolf corals, we applied the Sr/Ca-SST calibration ($m = -0.057 \pm 0.001$; $b = 10.658 \pm 0.025$) from weighted least squares (WLS) regression of the WLF10-03 and WLF10-10 composite record against OISST between May 1987-March 2010 (Jimenez et al., 2018). The composite calibration was utilized to standardize the calibrations across cores; however, the same results were found when using core-specific calibrations for the modern corals, as the calibration equations were similar between cores (Jimenez et al., 2018). For the Davies Reef, GBR corals, we used the Sr/Ca-SST calibration obtained from local calibration with in-situ temperature data (M. T. McCulloch et al., 2017):

$$Sr/Ca_{\text{coral}}(\text{mmol/mol}) = -0.046 \times SST + 10.12. \quad (1)$$

176 For both sites, the Li/Mg-SSTs were calculated using the calibration curve of Montagna et al. (2014).
 177 All new trace elemental geochemical data are shown in Figs. 4 and S9-S10.

178 **Determination of calcifying fluid pH and carbonate chemistry from boron system-** 179 **atics**

180 The boron in the remaining 400 μL aliquot of dissolved powder (after trace elemental analysis,
 181 above) was purified by ion exchange chromatography (after M. T. McCulloch et al., 2014), and the
 182 $\delta^{11}\text{B}$ was measured by MC-ICP-MS using a NU Plasma II at the University of Western Australia. The
 183 measured isotopic ratio of ^{11}B and ^{10}B of the carbonate samples were expressed relative to that of
 184 the NIST SRM 951 boric acid standard, in standard delta notation (in units of per mil or ‰):

$$\delta^{11}B_{\text{carb}} = \left[\frac{^{11}\text{B}/^{10}\text{B}}{^{11}\text{B}/^{10}\text{B}_{\text{standard}}} \right] \times 1000. \quad (2)$$

186 Reproducibility for the JCP-1 interlaboratory standard across these runs (2σ ; $n = 29$) was \pm
 187 0.22 ‰. Further, the long-term laboratory JCP-1 value and reproducibility of 24.36 ± 0.34 ‰ (2σ);

188 $n = 101$; see also J. D’Olivo & McCulloch, 2017) agree well with reported values with and without
 189 oxidative pre-treatment (Gutjahr et al., 2021). Therefore, although the analytical uncertainty of our
 190 results may be slightly higher because the samples were not pre-cleaned (Gutjahr et al., 2021), the
 191 reported values are well within error of the pre-cleaned values from Gutjahr et al. (2021). The 2σ
 192 uncertainties in this study are on par with that of pre-cleaned samples ($n = 29$), while the long-term av-
 193 erage falls between that of published values with and without cleaning ($n = 101$). Finally, previous
 194 work suggests that $\delta^{11}\text{B}$ is relatively insensitive to sample cleaning methods (Holcomb et al., 2015).

195 We used paired boron isotope and B/Ca ratios to determine the pH and carbonate ion concen-
 196 tration, leveraging three key features of boron isotope systematics (as reviewed by DeCarlo et al., 2018;
 197 Thompson, 2021). First, boron speciation in seawater depends strongly on pH, with borate ion ($\text{B}(\text{OH})_4^-$)
 198 dominating at higher pH and boric acid ($\text{B}(\text{OH})_3$) dominating at lower pH ($< \sim 8.5$). Second, boron
 199 isotopes are strongly fractionated between the two species, with a $+27\%$ offset between borate and
 200 boric acid. Taken together, as pH decreases, the fraction of boron as borate decreases and the $\delta^{11}\text{B}$
 201 increases. Third, as corals calcify from a semi-isolated calcifying fluid, borate may substitute for the
 202 carbonate ion (CO_3^{2-}) (Sen et al., 1994). Although there are multiple pathways by which this could
 203 occur, recent inorganic precipitation studies (Holcomb et al., 2016) suggest that it likely occurs via
 204 de-protonation and co-precipitation with CO_3^{2-} (Noireaux et al., 2015), rather than via bicarbonate
 205 or some mixture of the two, as previously proposed (Allison et al., 2014).

206 The initial calcifying fluid $\delta^{11}\text{B}$ and total boron concentrations are thought to be the same as that
 207 of seawater, as seawater serves as the source of boron; further, the boron isotopic composition and con-
 208 centration remains relatively constant during calcification, due to low partitioning coefficient (K_D) of
 209 B/Ca between aragonite and seawater (i.e., B is strongly excluded from the skeleton during precip-
 210 itation, Holcomb et al., 2016). We note that diffusion may violate these assumptions under certain
 211 conditions; for example, diffusion of isotopically distinct boric acid may alter the $\delta^{11}\text{B}$ relative to sea-
 212 water (Gagnon et al., 2021) or increase boron concentrations relative to seawater when pH is elevated.
 213 However, there is no experimental evidence for these confounding factors within tropical, symbiont-
 214 bearing coral species; as symbionts provide an additional critical source of DIC to the calcifying fluid,
 215 biomineralization processes in symbiont-bearing corals are markedly different from that of the cold-
 216 water species for which these limitations have been identified. We therefore follow the approach of other
 217 recently published studies in this regard (Chalk et al., 2021; DeCarlo et al., 2018; J. P. D’Olivo et al.,
 218 2019; Ross et al., 2019, 2017; M. T. McCulloch et al., 2017).

219 As a result of these processes, the skeletal $\delta^{11}\text{B}$ reflects the pH of the calcifying fluid (pH_{cf}), while
 220 the [B] reflects both pH and the $[\text{CO}_3^{2-}]$ (Holcomb et al., 2016; DeCarlo et al., 2018). We calculate
 221 pH_{cf} from $\delta^{11}\text{B}$ of the carbonate skeleton (after Zeebe & Wolf-Gladrow, 2001):

$$222 \quad \text{pH}_{cf} = \text{p}K_B - \log \left[\frac{(\delta^{11}B_{sw} - \delta^{11}B_{carb})}{(\alpha_{(B3-B4)}\delta^{11}B_{carb} - \delta^{11}B_{sw} + 1000(\alpha_{(B3-B4)} - 1))} \right], \quad (3)$$

223 where the $\delta^{11}\text{B}$ of seawater ($\delta^{11}\text{B}_{sw}$) was defined as 39.61% (Foster et al., 2010), the boron iso-
 224 tope equilibrium constant ($\alpha_{(B3-B4)}$) was set to 1.0272 (Klochko et al., 2006), and the dissociation con-
 225 stant of boric acid ($\text{p}K_B$) was calculated from temperature, salinity and pressure (after A. G. Dick-
 226 son, 1990). To standardize methods across cores (as *in situ* data is not available for all sites or time
 227 periods), we used Li/Mg-derived SSTs and Simple Ocean Data Assimilation (SODA) sea-surface salin-
 228 ity (SSS). We used mean climatological SODA SSS (33.5 PSU) for fossil analyses (prior to the indus-
 229 trial era).

230
231
232

Empirical constraints on the B/Ca partitioning coefficient between aragonite and seawater and its dependency on pH_{cf} (Holcomb et al., 2016) permit reconstruction of carbonate ion concentration in the calcifying fluid from paired $\delta^{11}\text{B}$ - pH_{cf} and B/Ca measurements (DeCarlo et al., 2018):

233

$$K_D \equiv (\text{B/Ca})_{\text{CaCO}_3} \times \frac{[\text{CO}_3^{2-}]_{\text{cf}}}{[\text{B}(\text{OH})_4^-]_{\text{cf}}}, \quad (4a)$$

234
235

$$K_D = 0.00297 \exp(-0.0202[\text{H}^+]_{\text{cf}}), \quad (4b)$$

237 and

238

$$[\text{CO}_3^{2-}]_{\text{cf}} = \frac{K_D \times [\text{B}(\text{OH})_4^-]_{\text{cf}}}{(\text{B/Ca})_{\text{CaCO}_3}}, \quad (5)$$

239
240
241
242
243

where Eq. 3b follows the formulation of (M. T. McCulloch et al., 2017). Although there continues to be debate over the best K_D formulation (DeCarlo et al., 2018), Eq. 3b is likely to be most accurate for tropical reef-building corals as it does not include the (Mavromatis et al., 2015) experimental data, which was collected from NaCl solutions (rather than seawater) at very low $[\text{CO}_3^{2-}]$ relative to that of coral CF.

244
245
246
247
248
249
250
251
252
253
254
255
256
257
258
259
260
261
262

As reviewed by (DeCarlo et al., 2018), uncertainties still remain with regards to the most accurate formulation for K_D and the degree to which Ca^{2+} is upregulated within the cf. We evaluated the sensitivity of our results (see Figure S6-7, S10, S14) to the K_D formulation, following the equations of Holcomb et al. (2016); M. T. McCulloch et al. (2017); DeCarlo et al. (2018) and the boron systematics package of DeCarlo et al. (2018), as well as using a constant K_D of 0.002 (after Allison, 2017). Our sensitivity tests show that these uncertainties only marginally impact the absolute magnitude of inferred DIC_{cf} and do not influence the relative changes across sites and time periods (the focus of this work). Further, the inferred DIC_{cf} upregulation is higher using the K_D formulation of M. T. McCulloch et al. (2017) (Figure S6); therefore, our chosen approach produces the most conservative change in DIC_{cf} and Ω_{cf} under warming and acidification. We similarly test the impact of Ca^{2+} upregulation relative to seawater on resulting Ω_{cf} calculations. For this, we use the mean and ± 1 standard deviation from these independent micro-sensor measurements of (see Sevilgen et al., 2019, Table 1). These sensitivity analyses demonstrate that uncertainties Ca^{2+} impact the absolute magnitude of Ω_{cf} within colonies (Figure S8), but not the relative differences among colonies, sites, or time periods (the focus of this study). We therefore utilize the most conservative approach, and report results using a Ca^{2+} scaling factor of 1, which is the lower (-1σ) bound from from Sevilgen et al. (2019). Inferred trends in Ω_{cf} and calcification would be greater if a constant K_D or higher Ca^{2+} are assumed (Figure S14). Therefore, the results reported here are the most conservative estimate of inferred Ω and calcification changes from preindustrial to modern conditions.

263
264
265
266
267
268
269
270

DIC_{cf} is calculated from the pH_{cf} (Eq. 2) and $[\text{CO}_3^{2-}]_{\text{cf}}$ using CO2SYS software (Lewis et al., 1998) and the following constants: carbonate species dissociation (from A. Dickson & Millero, 1987; Mehrbach et al., 1973), borate and sulfate dissociation (A. G. Dickson, 1990), and aragonite solubility (Mucci, 1983). Finally, we explore the relationship between pH, DIC and Ω of the coral calcifying fluid and Sr/Ca-SST (note: we utilize Sr/Ca-SST as a quasi-independent SST estimate rather than Li/Mg-SST, as the latter was used in Eq. 2). Our findings are robust to the paleo-thermometer used to assess the impact of temperature on coral carbonate chemistry (e.g., Fig. S8; see supplemental information).

271 Stable Isotope Geochemistry

272 Stable oxygen and carbon isotope ratios ($\delta^{18}\text{O}$ and $\delta^{13}\text{C}$) were analyzed on a Thermo Delta V
 273 Plus mass spectrometer, coupled to a Kiel IV carbonate preparation system, in the PACE lab, at the
 274 University of Michigan's Earth and Environmental Sciences department. Analyses were performed on
 275 splits of the same powders analyzed for trace elemental chemistry and paired $\delta^{11}\text{B}$ -B/Ca boron sys-
 276 tematics. Long-term analytical precision (1 sd) of Luxor internal carbonate standard was 0.08‰ for
 277 $\delta^{18}\text{O}$ and 0.05‰ for $\delta^{13}\text{C}$. All new stable isotope data are shown in Figs. 4 and S10.

278 Statistical analysis

279 Ordinary least squares regressions (OLS) were used to assess relationships among geochemical
 280 parameters within and among coral colonies, and in upregulation with respect to seawater conditions.
 281 First, OLS regressions were performed among reconstructed calcifying fluid and skeletal geochemi-
 282 cal parameters (Figs. 2, S1, S3-S6). ANCOVA and multiple comparisons were then utilized to assess
 283 differences in the relationship among groups (i.e., among individual cores, or among fossil Wolf, mod-
 284 ern Wolf, and GBR corals). Finally, OLS was utilized to assess the relationship between average up-
 285 regulation of pH_{cf} , DIC_{cf} , and Ω_{cf} and seawater chemistry and temperature. Confidence intervals (95%
 286 CI) were determined from the 5th and 95th percentiles of 1000 random draws of the distribution of
 287 upregulation estimates (based on the standard deviation and mean of each record).

288 Coral densitometry and calcification

289 Skeletal density was measured using a quantitative X-ray scanning method developed at the Aus-
 290 tralian Institute of Marine Science (Anderson et al., 2017, supplementary methods) alongside six com-
 291 pressed *Porites* sp. powder standards. These standards were used to calibrate X-ray grayscale val-
 292 ues to known density, by applying a linear fit between known density (multiplied by thickness) and
 293 the natural log of each standard's mean grayscale value. Grayscale values were measured from the background-
 294 corrected X-ray positives using Fiji software. Analytical precision of these X-ray density measurements
 295 was estimated using an additional standard with a known density (2.3977 g cm⁻²) and thickness (6.86
 296 mm) with values within the typical range of massive *Porites* spp. coral slabs. The average density of
 297 this quality control standard across all five X-rays used in this study was 2.3655 g cm⁻²; thus, we re-
 298 port an uncertainty of 0.043 g cm⁻² or 1.8%.

299 For each core, grayscale values were measured along 4 mm-wide transects on either side of the
 300 geochemical transect. We report density values from each transect, as well as the average across both
 301 transects (to account for micro-scale variations in density associated with skeletal architecture). For
 302 each transect, density was calculated using the standard calibration curve, normalized by slab thick-
 303 ness. Thickness was measured at 0.125 cm increments along two transects, and the average thickness
 304 was interpolated to 0.005 cm (the sampling resolution of the X-ray density measurements).

305 Annual growth metrics (density, extension, and calcification) were calculated from warm sea-
 306 son to warm season using annual tie points (Sr/Ca minima, SST maxima). This approach was uti-
 307 lized as the seasonal cycle was more clearly identifiable in the Sr/Ca series (relative to that of the growth
 308 series). Extension was calculated as the distance between successive Sr/Ca minima, and calcification
 309 as the product of extension and annual average skeletal density.

310 Seawater Carbonate System

311 Seawater carbonate chemistry (TCO_2 , Total Alkalinity [TA], pCO_2 , pH, and Ω_{arag}) were obtained
 312 from (D. P. Manzello, 2010; D. P. Manzello et al., 2014; Humphreys et al., 2018). Briefly, seawater
 313 samples were collected during the cool ($n = 24$) and warm ($n = 21$) seasons over multiple years in 500
 314 mL borosilicate glass bottles from 7 study sites throughout the archipelago: (1) Bartolomé, Santiago
 315 Island; (2) Santa Fe Island; (3) Punta Bassa, San Cristóbal Island; (4) Punta Pitt, San Cristóbal Is-
 316 land; (5) Devil’s Crown, Floreana Island; (6) Gardner Bay, Española Island; and (7) Darwin Island
 317 ($N=7$; summary statistics obtained from Humphreys et al., 2018). Here, we utilize the mean (\pm stan-
 318 dard error of the mean, SEM) values to assess the relationship between pH_{cf} and DIC_{cf} (calculated
 319 from paired coral $\delta^{11}\text{B}$ and B/Ca) and regional changes in the seawater CO_2 system. However, avail-
 320 able measurements are discrete, disjointed snapshots, and therefore lack temporal information with
 321 which to identify variability on interannual and longer timescales. Further, Ω_{arag} at Wolf Island is ex-
 322 pected to display higher mean values and lower seasonal variability (see D. Manzello, 2009, Fig. 1)
 323 than the seawater collection sites of (D. P. Manzello, 2010), as upwelling and equatorial undercurrent
 324 (EUC) strength and variability are weaker at Wolf Island. As values from Wolf Island are not pub-
 325 licly available, analyses were performed using both the in situ data from Darwin Island (D. P. Manzello
 326 et al., 2014; Humphreys et al., 2018) and Community Earth System Model version 1 (CESM1).

327 Community Earth System Model Biogeochemistry

328 Given the sparse network of seawater inorganic carbon measurements (i.e., DIC, pH, alkalinity)
 329 with which to calculate seawater aragonite saturation state, we use the CESM1 Last Millennium En-
 330 semble (LME, Otto-Bliesner et al., 2016) and Large Ensemble (LE, Kay et al., 2015) to compare the
 331 chemistry of the coral calcifying fluid to that of local seawater. This approach facilitates comparison
 332 across sites, as well as among 18th century (LME), 20th century (LME and LE), and end of 21st cen-
 333 tury (LE) conditions. The CESM1 marine ecosystem-biogeochemical module (Hurrell et al., 2013) per-
 334 mits analysis of the entire carbonate systems across space and time, permitting the first multi-site,
 335 multi-century synthesis of coral calcifying fluid chemistry in response to changing ocean conditions.

336 The CESM1 LME simulation was validated against OISST SSTs (Reynolds et al., 2007, Fig.
 337 S2), Simple Ocean Data Assimilation (SODA) SSS (Carton & Giese, 2008, not shown), buoy data
 338 (Sutton et al., 2019), seawater samples described above (Table S3), and the spatially interpolated cli-
 339 matology (1972-2013) from GLODAP version 2 (Lauvset et al., 2016, Table S3). CESM1 simulated
 340 pH and calculated Ω_{sw} compare well with the observations across the tropical Pacific, with differences
 341 of less than 0.05 and < 0.5 (RSDs of < 0.6 and 8%), respectively (Table S3). Further, these discrep-
 342 ancies may be at least partially attributed to the comparison of discrete in-situ snapshots of ocean
 343 pH with the climatological value over different baseline periods (over which there is a decreasing trend
 344 across the tropical Indo-Pacific).

345 We calculate Ω_{sw} from CESM1 LME (full forcing scenario) and LE (Representative Concentra-
 346 tion Pathway; RCP8.5) simulated SST, SSS, pH, and DIC using CO2SYS (as described above). Com-
 347 bining the simulated seawater pH, DIC, and Ω with boron-derived estimates of coral calcifying fluid
 348 pH, DIC, and Ω , we estimate the percentage upregulation of calcifying fluid geochemistry. For exam-
 349 ple, the percent change (henceforth “Pchange”) in aragonite saturation is calculated as:

$$350 \text{Pchange}_{\Omega} = \frac{\Omega_{\text{cf}} - \Omega_{\text{sw}}}{\Omega_{\text{sw}}} \times 100, \quad (6)$$

where Ω_{sw} represents the average over the time period overlapping each coral record from CESM1 LME and/or LE.

We perform sensitivity tests at the GBR site, where an *in-situ* seawater timeseries is available, to show that CESM1 LME and LE reproduce the observed $Pchange_{\Omega}$ (i.e., relative to seawater observations) to within $\pm 26\%$ (LME) and $\pm 0.5\%$ (LE), respectively (Table S8). Much of the discrepancy between LME and observed $Pchange$ can be attributed to differences in the time periods of coverage. Therefore, two sensitivity tests were used to assess: (i) the impact of using the annual average, seasonal average (cold vs. warm season), or monthly seawater value, and (ii) the impact of using the LME projected values versus using the LE values over the post-2005 interval (i.e., after the final year of the LME). Because the $Pchange$ seasonal variability is dominated by the variability in the coral calcifying fluid (which is \gg seawater variability), these sensitivity tests demonstrate that there is no difference in the mean $Pchange$ if the average seawater value is used in place of the observed temporal evolution of *in situ* Ω_{sw} (M. T. McCulloch et al., 2017). Further, this approach generates the most conservative estimate of the $Pchange$ variability at each site (i.e., $1\sigma = 23\%$ & 32% ; Table S8). The second sensitivity test demonstrated that LE-simulated seawater values displayed the best match with the *in situ* data over the post-2005 period ($\Delta Pchange_{\Omega} < 0.5\%$). Although there are no contemporaneous seawater samples collected near Wolf Island, Ω $Pchange$ values using seawater data from nearby Darwin (collected in June 2012) are within the 1σ range ($\pm 29\%$) of the CESM1-based estimates for WLF10-10a (ending in 2010, Table S9). We therefore conservatively reported an uncertainty of $\sim \pm 30\%$ for all $Pchange_{\Omega}$ estimates.

We also apply the method of (J. P. D’Olivo et al., 2019) to deconvolve the relative contribution of thermodynamics (i.e., SST-driven changes in calcification and/or buffering capacity, Guo, 2019) and pH_{sw} in the observed pH_{cf} trends and seasonal variability. Briefly, we performed a multivariate linear regression between CESM1 simulated temperature and pH_{sw} (independent predictors) and pH_{cf} (dependent predictand). The sensitivity of Wolf coral pH_{cf} to SST and pH_{sw} can be expressed as:

$$pH_{cf} = 0.26 \times pH_{sw} - 0.0019 \times SST + 6.34, \quad (7)$$

Similar results were obtained when Sr/Ca-SSTs we used in place of CESM1 simulated SSTs. To quantify the role of SST and pH_{sw} in the observed trends (WLF10-10 and fossil vs. modern) and seasonal variability, we model pH_{cf} from Eq. 6 using either (1) the average pH_{sw} and simulated SST, or (2) the average SST and simulated pH_{sw} , respectively.

Predicted changes in coral calcification

Finally, we use the IpHRAC model from (M. McCulloch et al., 2012) to predict the changes in calcification rate (G) from Ω_{cf} between time periods (i.e., 18th and 20th):

$$G = k \times (\Omega_{cf} - 1)^n, \quad (8)$$

where

$$k = -0.0177 \times SST^2 \quad (9)$$

and

$$n = 0.0628 \times SST + 0.0985. \quad (10)$$

389 Ω_{cf} is calculated from simulated pH, Ω_{sw} , SST, and SSS and the Pchange (%) upregulation,
 390 as described above. Calcification rates are reported as percent changes relative to the baseline
 391 period (1970-2005, unless otherwise noted).

392 Results and Discussion

393 Seasonal pH, DIC and Ω of coral calcifying fluid

394 Here we compare new reconstructions of SST and calcifying fluid geochemistry (Table S-1) from
 395 modern and subfossil Galápagos coral cores with published reconstructions from the GBR (M. T. Mc-
 396 Culloch et al., 2017; Ross et al., 2017; J. P. D’Olivo et al., 2019). Two 18th century coral cores col-
 397 lected at Wolf Island show that as SST increases, pH_{cf} decreases (despite the regional pH_{sw} increase;
 398 Fig. S1a and 2a). The slope of this relationship (WLF04: -0.022 pH units per °C, $N = 33$, $r^2 = 0.52$;
 399 WLF05: -0.033 pH units per °C, $N = 45$, $r^2 = 0.43$; Figure S1) is nearly identical to that found among
 400 replicate modern corals from the GBR (Davies-02: -0.035 pH units per °C, $N = 50$, $r^2 = 0.82$; Davies-
 401 03: -0.020 pH units per °C, $N = 54$, $r^2 = 0.80$). The seasonal pH_{cf} change is also similar among GBR
 402 modern and the Wolf fossil coral, with a -0.03 to -0.06 unit change between the average warm and cold
 403 seasons (Table S2) and a range of 0.2 to 0.3 pH units at each site. However, the SST-pH relationship
 404 weakens in the two modern (20th century) Wolf corals, which display a reduced seasonal pH range (ΔpH
 405 = -0.003 to -0.02, Table S2) and a weaker relationship with temperature (i.e., a shallower slope and
 406 lower r^2) compared to fossil Wolf cores (Fig. S1a).

407 Comparing the modern and fossil data from Wolf, we demonstrate that the pH_{cf} -SST relation-
 408 ship is significantly weaker in the modern corals than in the fossil corals. In contrast, the Wolf fos-
 409 sil and GBR modern corals are not significantly different from one another (Figure 2a). The greater
 410 SST range in modern cores (Fig. 2a, x-axis) would by itself strengthen this relationship (as in J. P. D’Olivo
 411 et al., 2019) and therefore cannot explain the observed patterns; we therefore infer that the weaken-
 412 ing is likely driven by reduced pH upregulation (Fig. 3c-d), due to the impacts of OA and/or ther-
 413 mal stress (rather than by temperature-induced changes in calcification or buffering capacity alone
 414 Guo, 2019). The difference in slope between the fossil and modern corals equates to 7-40% difference
 415 in H^+ ions in the calcifying fluid (with larger changes at lower temperatures, Fig. 2a). As a result,
 416 Ω_{cf} displays a significant positive relationship with SST in modern Wolf corals (Figs. 2c, 3c-d), with
 417 up to 5% lower saturation during the cold season (September-November; SON) relative to the warm
 418 season (Table S2). In contrast, there is no relationship between Ω_{cf} and temperature in the fossil coral
 419 (Figs. 2c, 3a-b) and < 1.5% change in Ω_{cf} seasonally (Table S2), though we note that a significant Ω_{cf} -
 420 temperature relationship is observed in the WLF04 data alone (Fig. S1d). These results indicate that
 421 the fossil coral maintained a steady aragonite saturation state in its calcifying fluid across seasonally
 422 varying environmental conditions, while the modern Wolf corals did not. Put another way, modern
 423 Wolf corals appear to have partially lost their ability to buffer calcifying fluid chemistry against changes
 424 in seawater pH and Ω . This loss of buffering capacity—shown here for the first time—implies a loss of
 425 resilience that is likely to lead to reduced calcification under continued environmental change.

426 Reproducibility

427 The mean and seasonal-interannual variance in calcifying fluid geochemistry were broadly re-
 428 producible across cores from both periods (within and among cores at a single site; Table S2, Figure
 429 4, S1 & S10). However, an anomalously low $\delta^{11}\text{B}$ and B/Ca departure in core WLF05 co-occurring
 430 with a low-density and high Sr/Ca-SST anomaly in 1731-1732 emphasizes the need for further work
 431 to assess the impact of skeletal density, microstructure (Chalk et al., 2021), and transect quality (Reed
 432 et al., 2019, 2021) on skeletal geochemistry within a single colony. Such within colony variations are

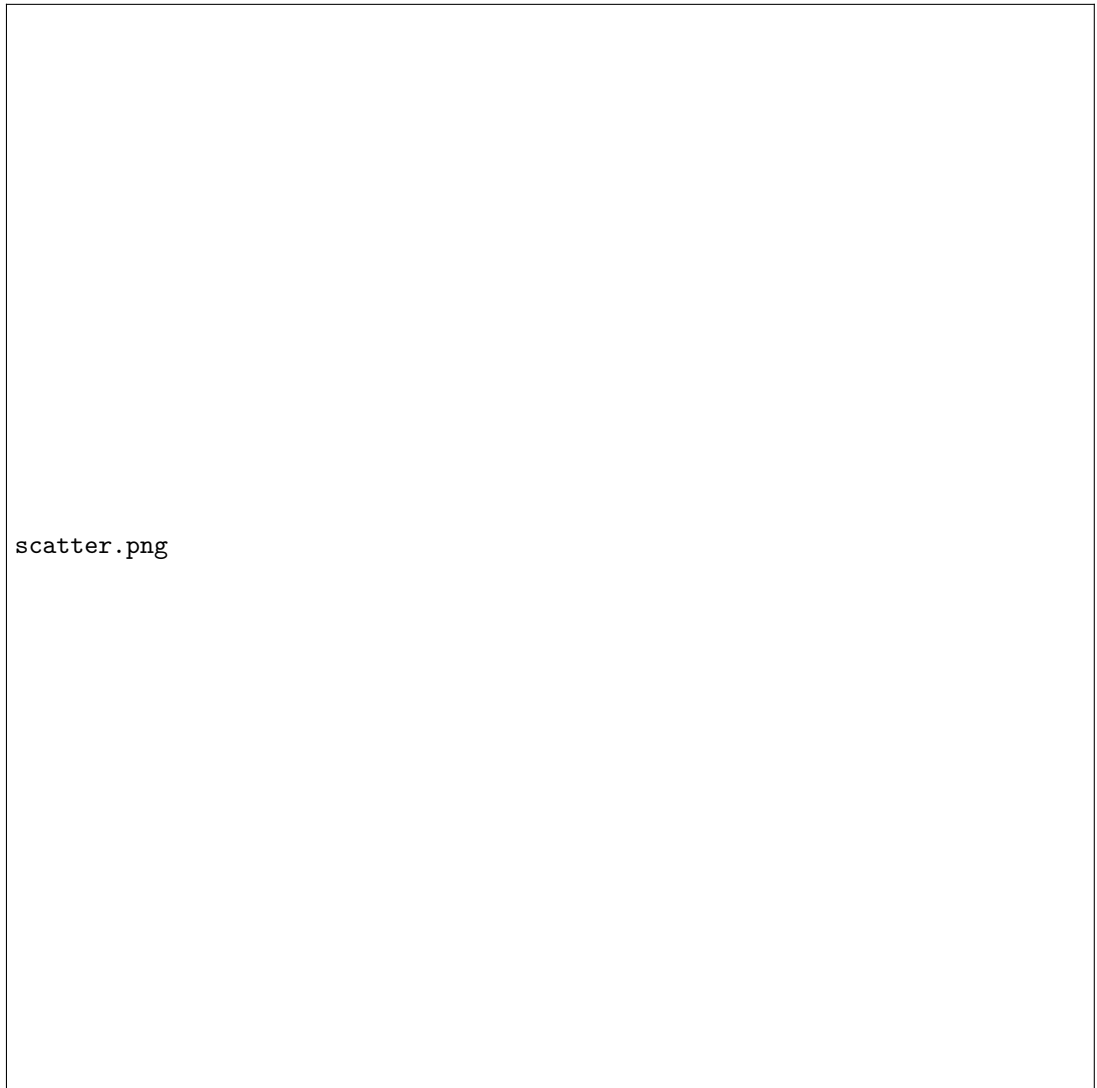


Figure 2. Comparison of the relationships among geochemical proxies (Box 1), Wolf 18th-century fossil (red squares) and modern (20th century, orange circles) versus Great Barrier Reef modern (blue circles): (a) Sr/Ca-SST vs. pH_{cf} , (b) Sr/Ca-SST vs. DIC_{cf} , (c) Sr/Ca-SST vs. Ω_{cf} , (e) DIC_{cf} vs. $\delta^{13}\text{C}$ (with and without flier outlined in gray), and (f) Sr/Ca vs. Mg/Ca. Comparison of the pre- 1997/98 thermal stress (blue), and post- 1997/98 thermal stress (red) Sr/Ca-SSTs vs. pH_{cf} for all modern coral data (black) is shown in (d). In all panels, roman numerals (I-III) denote that the slope of the relationship is significantly different from other groups, based on ANCOVA and multiple comparisons (where a significant difference among groups was identified). Groups with the same roman numeral are not significantly different from one another.



Figure 3. Schematic overview of the main seawater and physiological controls (cold season a,c; warm season b,d) on calcifying fluid and skeletal geochemistry in Galapagos 18th-century fossil (a-b) and modern (c-d) corals, identified in the current study. Figure 3 modified from (Thompson, 2021). Arrows indicate the sign of the change, with the thickness indicating the relative magnitude of the change; ‘—’ denote variables with limited to no change.

likely to be more severe at marginal reef sites like the Galápagos Islands, where corals are susceptible to boring bivalves and display lobate growth structure and complex microscale growth features, such as convergent corallite fans, changes in growth direction, and corallites angled relative to the sampling plane (Reed et al., 2021). Nevertheless, outside this short-lived anomaly, the geochemical relationships reported here were reproducible within replicate cores from a single Galápagos fossil coral colony, with no significant differences in slope between the replicate fossil cores (Fig. S1). The only exceptions were the slope of the relationship between $\delta^{13}\text{C}$ and DIC_{cf} (Fig. S1e) and the intercept of the DIC_{cf} -SST relationship (Fig. S1b)—suggesting that proxies for metabolic activity may be most susceptible to non-environmental or physiological factors (e.g., skeletal microstructures, overall transect quality, symbiont density and composition, and/or shading within colonies with complex 3D structures), as previously observed for $\delta^{13}\text{C}$ among transects. Nevertheless, the reproducibility of these relationships suggests that this approach can help expand our knowledge of calcifying fluid geochemistry prior to the industrial era.

Further, sensitivity tests demonstrate that the differences in pH and Ω upregulation across sites and time periods are robust regardless of the choice of K_{D} and $[\text{Ca}^{2+}]_{\text{cf}}$ (Figures S3-S5). Further, the values are within the range of those obtained through independent micro-sensor measurements (Sevilgen et al., 2019); recent work comparing $\delta^{11}\text{B}$ - and microelectrode-based pH_{cf} support the utility of $\delta^{11}\text{B}$ as a proxy for diurnally-averaged pH_{cf} (Guillermic et al., 2020).

Dissolved Inorganic Carbon & $\delta^{13}\text{C}$ variability

The controls on pH upregulation and DIC_{cf} likely differ across sites. In Australia, seasonal upregulation of pH_{cf} occurs in response to seasonal variations in temperature (Guo, 2019; J. P. D’Olivo et al., 2019), pH_{sw} (J. P. D’Olivo et al., 2019), and metabolic DIC availability (M. T. McCulloch et al., 2017), with lower DIC during the winter months due to reduced light and cooler temperatures (M. T. McCulloch et al., 2017). This mechanism was proposed in the GBR and Ningaloo Reef, Australia, where both DIC_{cf} (Figs. 2b and S1b) and $\text{DIC}_{\text{cf}}/\text{DIC}_{\text{sw}}$ display a strong positive relationship with temperature (M. T. McCulloch et al., 2017). This pH seasonality is consistent amongst a wide range of reefs, including the GBR, Coral Sea, Western Australia, Caribbean, and Central Pacific (Knebel et al., 2021; Hemming et al., 1998; Pelejero et al., 2005; M. T. McCulloch et al., 2017; J. D’Olivo & McCulloch, 2017; Ross et al., 2019; J. P. D’Olivo et al., 2019; Chalk et al., 2021). However, all of these sites have fundamentally different dynamics than in the Galápagos, where the cool season experiences upwelling of DIC-rich waters (Kessler, 2006, Fig. 3a-b) that impacts the seasonality of CF chemistry. As a result of these confounding DIC_{sw} and metabolic DIC signals, we find that DIC_{cf} is nearly independent of temperature in modern Wolf corals (Figs. 2b, 3c-d; though note a very weak positive relationship observed in core WLF03, Fig. S1) and displays a weak positive relationship with temperature in the Wolf fossil coral (Figs. 3a-b, S1). Further, DIC_{cf} is upregulated by a near-constant factor of ~ 2 relative to DIC_{sw} in modern Wolf corals, compared with a stronger, seasonally varying DIC_{cf} enrichment in GBR corals ($\text{DIC}_{\text{cf}}/\text{DIC}_{\text{sw}} = 2.2\text{-}3.2$, Table S2) and Galápagos fossil corals.

Comparison of the carbon isotopic ($\delta^{13}\text{C}$) variability among cores may explain why pH regulation is weaker in modern Wolf corals (Fig. 2e). First, a relationship between $\delta^{13}\text{C}$ and the DIC_{cf} in Wolf modern and fossil corals is weak or absent, suggesting that metabolic processes and upwelling contribute approximately equally to the carbon pool at this site. During the cool season, both metabolic processes (which preferentially remove light carbon, enriching the carbon pool and increasing skeletal $\delta^{13}\text{C}$; as reviewed by Swart, 1983) and upwelling (which contributes isotopically light carbon, decreasing skeletal $\delta^{13}\text{C}$) contribute to DIC_{cf} ; therefore the signals compensate, reducing $\delta^{13}\text{C}$ variance relative to that of DIC_{cf} (Fig. 3). Nevertheless, we note a weak negative relationship between $\delta^{13}\text{C}$ and DIC_{cf} in core WLF03 (Fig. S1), in addition to the consistently more negative $\delta^{13}\text{C}$ values in the modern samples from the burning of fossil fuels (“Suess effect”; Keeling, 1979). Although additional

480 data are needed to assess the complex interplay of DIC variability at this site, these results suggest
 481 that the upwelling of isotopically light carbon is increasingly dominating the DIC_{cf} pool as the sea-
 482 water DIC pool becomes isotopically lighter and the coral-algae symbiosis becomes increasingly stressed.
 483 Indeed, a significant relationship between $\delta^{13}\text{C}$ and DIC_{cf} is only present in the post 97/98 data (Fig-
 484 ure S6), driven primarily by large isotopically heavy, low DIC anomalies during and following ther-
 485 mal stress and bleaching.

486 To assess the strength of DIC upregulation, we use simulated values for seawater carbonate pa-
 487 rameters that are unavailable from coral proxies (see Methods), but that compare reasonably well to
 488 the limited available direct seawater observations at nearby locations, collected over disparate time
 489 periods (Table S3). We find that Galápagos modern DIC_{cf} never reaches above 2.2 times that of sim-
 490 ulated DIC_{sw} (DIC_{cf} max = 4654 $\mu\text{mol}/\text{kg}$ vs. DIC_{sw} max = 2091 $\mu\text{mol}/\text{kg}$; D. P. Manzello, 2010),
 491 whereas the fossil coral DIC_{cf} reaches as much as ~ 2.8 times that of seawater (5663 $\mu\text{mol}/\text{kg}$, which
 492 is within the range observed at the GBR, Fig. 2b). These results are consistent with a larger contri-
 493 bution of metabolic carbon to the DIC pool in the fossil coral (values DIC_{cf}/DIC_{sw} > 1), with large
 494 seasonal (Table S2) and interannual variability (Fig. 4e) in DIC_{cf} that reflects the relative strength
 495 of upwelling and photosynthetic carbon fixation in response to light and temperature. Further, the
 496 weak relationship between DIC_{cf} upregulation and Ω_{sw} across all Wolf corals (Table S4) suggests that
 497 this decrease in DIC_{cf} variability from pre-industrial conditions is likely driven primarily by dysbio-
 498 sis (i.e., bleaching or loss of healthy coral microbiome and thus a reduction in metabolic carbon) as-
 499 sociated with thermal stress, rather than OA. This is consistent with DIC_{cf}/DIC_{sw} departures of <
 500 1 (i.e., loss of metabolic carbon) during the 1997/98 thermal stress in both modern cores (equating
 501 to a 14-34% reduction in DIC upregulation, Fig. 4e). Similar reductions in DIC_{cf} upregulation are ob-
 502 served during other warm extremes in the modern record, whereas DIC upregulation is highest dur-
 503 ing warm periods in the fossil record. Our results therefore add to the growing body of work identi-
 504 fying adverse effects of thermal stress and bleaching on coral CF chemistry under ocean warming (J. D’Olivo
 505 & McCulloch, 2017; Schoepf et al., 2015, 2021; J. P. D’Olivo et al., 2019; Dishon et al., 2015; Che-
 506 ung et al., 2021). The changes in DIC upregulation identified here imply that extreme thermal stress
 507 undermines coral health via photosynthetic reductions that coincide with weak upwelling (and thus
 508 feeding capacity); together, these changes deprive the colony of the energy needed to drive the Ca-
 509 ATPase pump and/or other active pathways (e.g., other alkalinity pumps or paracellular transport)
 510 that upregulate pH_{cf}, leaving them more susceptible to regional changes in DIC_{sw} and pH_{sw}.

511 Taken together, these results suggest that DIC_{cf} variability in Wolf corals reflects a complex sea-
 512 sonal interplay between upwelling (cold, high DIC_{sw}, low $\delta^{13}\text{C}_{\text{DIC}}$; May-Nov cold season) and pho-
 513 tosynthetic / metabolic (warm, high DIC_{cf}, high $\delta^{13}\text{C}_{\text{cf}}$; Dec-April warm season) processes, the lat-
 514 ter of which contributes less to the carbon pool in modern Wolf corals. Regional upwelling elevates
 515 both concentrations and variability of DIC_{sw}; these combine with the coral’s metabolic variations to
 516 produce fundamentally different DIC_{cf} dynamics at this site relative to the GBR. In other words, in
 517 Galápagos corals, pH upregulation is partly driven by variations in the seawater carbon pool, rather
 518 than changes in metabolic pathways alone. We thus find that seasonal pH_{cf} variations at Wolf (Ta-
 519 ble S2) are driven primarily by seasonal temperature and pH_{sw} variability (e.g., 73% and 33%, respec-
 520 tively, in the longest core WLF10-10; after J. P. D’Olivo et al., 2019, see Methods). These results im-
 521 ply that Galápagos corals are more sensitive to environmental drivers, whereas metabolic processes
 522 can regulate cf chemistry more strongly in GBR corals.

523 Temporal variability in pH_{cf} & impact of thermal stress

524 Comparing the temporal evolution of pH_{cf} among GBR and Wolf corals over the late 20th cen-
 525 tury supports our interpretation that corals experience difficulty upregulating pH_{cf} as seawater con-

526 ditions become less favorable. First, modern Wolf corals display an abrupt drop and subsequent rise
 527 in pH_{cf} during and following the 1997/98 El Niño event (Fig. 4a), respectively; this event was char-
 528 acterized by extreme temperature anomalies (Jimenez et al., 2018; Cheung et al., 2021) (Fig. 4g), stress
 529 and bleaching (P. Glynn, 2001). The decrease in pH_{cf} (towards ambient values) likely resulted from
 530 a combination of the loss of metabolic DIC from symbiotic photosynthesis (weakening the ability of
 531 corals to regulate their internal pH via the Ca-ATPase or other alkalinity pumps), temperature-induced
 532 changes in buffering capacity, and the bleaching-related reduction in calcification rate. The latter is
 533 supported by the greater change in pH_{cf} in core WLF-3, in which calcification rate declined by 26%
 534 in 1998 (Fig. S7). In turn, these changes impact Ω_{cf} regulation (Fig. 2c and S6d) and calcification,
 535 and thus the imprint of Rayleigh fractionation on the widely utilized Sr/Ca-SST proxy (with less frac-
 536 tionation following bleaching, suggesting a slowdown in calcification, Fig. S6h), though Cheung et al.
 537 (2021) demonstrate that the Sr/Ca-SST record at this site is not likely to be influenced by these pro-
 538 cesses. Therefore, although our results are reproducible among proxy-based and observational SST
 539 data (Figure S8-9), the breakdown of pH upregulation in modern corals (particularly post-thermal
 540 stress and bleaching) may be even greater than indicated by the Sr/Ca-SST proxy records (see Sup-
 541 plemental Text, Figure S8).

542 The full suite of geochemical tracers measured in modern Galápagos corals provides additional
 543 support for the thermal sensitivity of active transport pathways (Ca-ATPase pump, other alkalinity
 544 pumps, and/or paracellular transport), particularly following the 1997/98 El Niño event (see supple-
 545 mentary text; Figs. S6 and S10). Departures in U/Ca, Mg/Ca, and $\delta^{13}\text{C}$ suggest changes in $[\text{CO}_3^-]$,
 546 Rayleigh fractionation, active transport, and photosynthetic activity following acute thermal stress
 547 that are consistent with our interpretations from reconstructed Sr/Ca-SST, DIC_{sw} , and pH (see sup-
 548 plemental text). For example, the relationship between Sr/Ca and both Mg/Ca and U/Ca weakens
 549 significantly after 1997/98, implying weaker Rayleigh fractionation and/or reduced active transport.
 550 A weakening of the pH_{cf} -SST relationship after 1997/98 (Figs. 2d and S6a) also supports the hypoth-
 551 esis that corals lose their ability to regulate pH_{cf} via the Ca-ATPase pump or other active pathways
 552 post-stress. However, our results are based on relatively few data following this stress event, limiting
 553 the significance of these changes (Fig. S6a); similar analyses of additional stress events would clar-
 554 ify these patterns and improve interpretations of calcification and skeletal geochemistry following ther-
 555 mal stress and bleaching. Nevertheless, these results are consistent with other recent studies demon-
 556 strating acute impacts of thermal stress on pH_{cf} and skeletal geochemistry (M. T. McCulloch et al.,
 557 2017; Ross et al., 2017; J. D’Olivo & McCulloch, 2017; J. P. D’Olivo et al., 2019; Guillermic et al.,
 558 2020; Clarke et al., 2017, 2019; Schoepf et al., 2021; Cheung et al., 2021).

559 Limits to calcifying fluid homeostasis

560 To understand how corals will respond to ongoing and future environmental changes, it is crit-
 561 ical to assess the capacity of corals to regulate Ω_{cf} across sites and time periods with different base-
 562 line seawater chemistry. Here, we demonstrate that despite large changes in seawater chemistry be-
 563 tween the 18th century and modern periods inferred from model simulations (Fig. 1c), there is no re-
 564 lationship between Ω_{sw} and the upregulation of Ω_{cf} in Galápagos corals (Table S4). In other words,
 565 Ω_{sw} has not had a detectable influence on upregulation capacity, implying that Galápagos corals have
 566 not adapted their capacity to regulate Ω_{cf} in response to thermal extremes and OA since the pre-industrial
 567 era. Therefore, although they continue to regulate their internal growth environment at maximum ca-
 568 pacity, the resulting calcifying fluid saturation levels are significantly lower in modern corals due to
 569 OA (Fig. 3c-d vs. 3a-b).

570 Our results contrast with the apparent pH “homeostasis” observed in extreme environments (near
 571 submarine seeps in Papua New Guinea (Wall et al., 2016) and Puerto Morelos, Mexico (Wall et al.,



Figure 4. Time series of boron-derived calcifying fluid geochemistry, Sr/Ca-SSTs, and skeletal density: Wolf 18th-century fossil (red) and modern (20th century, orange) versus Great Barrier Reef (blue). (a) $\delta^{11}\text{B}$ (permil), (b) B/Ca ($\mu\text{mol/mol}$), (c) pH_{cf} (total scale), (d) DIC_{cf} ($\mu\text{mol/kg}$), (e) Ω_{cf} , (f) Percent upregulation of pH_{cf} with respect to pH_{sw} (%), (g) Percent upregulation of DIC_{cf} with respect to DIC_{sw} (%), (h) Percent upregulation of Ω_{cf} with respect to Ω_{sw} (%), (i) Sr/Ca-SSTs ($^{\circ}\text{C}$), and (j) skeletal density (g/cm^3). See Methods for how these parameters were derived from proxy and model data. Gray shading depicts the range of 18th-century fossil values; red shading depicts warm anomalies associated with the 1997/98 El Niño event; mean values are denoted by dotted lines on each series.

2019) and in the Heron Island (GBR) FOCE (Georgiou et al., 2015). At these $p\text{CO}_2$ extremes, *Porites* spp. corals show a strong relationship between Ω_{cf} upregulation and seawater conditions (e.g., $\Delta\Omega_{\text{cf}}$ of 214% and 270% per unit change in Ω_{sw} , respectively, Table S4). However, in both scenarios, Ω_{sw} was 19-82% lower than observed on any modern reefs studied here. Further, seep corals have persisted in these conditions for multiple generations and likely have acclimatized and/or adapted to low seawater saturation over long time periods. Therefore, such sites are unlikely to be good analogues for adaptation potential to current rates of OA, which can occur over the lifetime of an individual coral (100+ years). Therefore, despite the potential for acclimation indicated by such studies of extreme conditions, under the real-world environmental change and multivariate stresses, Galápagos *Porites* spp. corals have not demonstrated an ability to adapt to changing pH via pH_{cf} upregulation.

Our synthesis of modern and fossil corals living under contrasting seawater conditions suggests that there may be a physiological limit to the capacity of corals to upregulate pH_{cf} in response to changing ocean conditions and fluctuations in DIC_{cf} . The capacity of corals to upregulate Ω_{cf} is therefore likely to be dictated (to the first order) by their capacity to upregulate DIC_{cf} via metabolic processes (e.g., GBR corals, particularly in the summer months), which we show is reduced both at marginal sites and following bleaching. Galápagos corals, which have low DIC_{cf} despite high regional DIC_{sw} , therefore require greater pH_{cf} upregulation than modern GBR *Porites* spp. corals to maintain similar rates of calcification; the limited capacity to upregulate pH_{cf} has therefore reduced Ω_{cf} under modern conditions. Such a physiological limit, if it holds across future acidification (and across additional sites), is likely to leave corals in low-pH, high-DIC environments (i.e., in marginal environments) particularly susceptible to changing ocean saturation.

At both sites, the degree of pH_{cf} , DIC_{cf} , and Ω_{cf} upregulation relative to seawater varied in concert with SST; warm seasons or years experience greater Ω_{cf} and DIC_{cf} upregulation, and weaker pH_{cf} upregulation (Table S2 & S5; Fig. 4d-g). These results agree with previous work showing a strong relationship between pH_{cf} upregulation and temperature across a latitudinal gradient (Ross et al., 2019). Physicochemical modeling of coral cf chemistry suggests the temperature dependence of pH upregulation is driven primarily by calcification kinetics, and secondarily by seawater buffering capacity (i.e., the sensitivity of the pH_{cf} to changes in total alkalinity; Guo, 2019). This dependence is particularly apparent during the 1997/98 El Niño in Wolf modern corals, with anomalously high pH_{cf} and high Ω_{cf} relative to seawater during and immediately following peak warming (January 1998 to September 1998), potentially due to increased buffering capacity at higher temperatures. However, the increase in pH_{cf} upregulation following peak warming (i.e., during the stress recovery period) implies that other physiological mechanisms must also be at play, such as a change in the refresh rate of the cf or a change in the balance of bicarbonate and carbonate that is transported to the site of calcification (J. D’Olivo & McCulloch, 2017). Although uncertainties in the fidelity of the Sr/Ca-SST proxy across this thermal stress event may add uncertainty to the SST signal (J. D’Olivo & McCulloch, 2017), only ~2% of the pH_{cf} anomaly can be explained by SST alone, and the Ω upregulation anomaly (i.e., 97/98 $\Delta\Omega$ relative to the colony mean $\Delta\Omega$, Fig. 4h) is robust between the replicate modern cores (23 and 31%) despite differences in calcification rate between colonies. Nevertheless, similar Ω upregulation anomalies does not preclude differences in the relative roles of DIC_{cf} and pH_{cf} in this saturation change (Fig. 4). Our results suggest that although the response of metabolic carbon production and/or pH_{cf} to thermal stress varies from colony to colony, the relative change in Ω_{cf} with respect to seawater does not vary significantly among colonies. Again, these results demonstrate strong physiological limits to the corals’ ability to regulate their internal carbonate chemistry, and that this limit is likely an emergent property resulting from the interplay of numerous physiological processes or pathways.

618 Implications for calcification under warming & acidification

619 Our results demonstrate that physiological limitations have already had a pronounced impact
 620 on the geochemistry of the calcifying fluid in Galápagos *Porites* sp. corals. The pH_{cf} declined signif-
 621 icantly between 18th century and modern Wolf corals ($Z = 24.3$, $N = 108,277$, $p < 0.001$), and from
 622 1975 to 2010 in the long modern Wolf (GW10-10) record (with a trend of -0.18 pH units per decade).
 623 Over 99.9% of this recent trend (between 1975 and 2010) can be attributed to pH_{sw} , with warming
 624 contributing less than 0.3% (after J. P. D’Olivo et al., 2019, see methods). The mean pH_{cf} was 8.57
 625 in two 18th century fossil cores from one colony ($N = 78$) and 8.50 in the two modern corals ($N = 203$,
 626 Fig. 4, Table 1). This pre-industrial to modern mean pH_{cf} difference can be attributed some combi-
 627 nation of pH_{sw} or SST changes. A large model ensemble of simulated changes between these periods
 628 suggests that either pH_{sw} or SST could produce pH_{cf} changes of 0.06-0.07 (see methods). In contrast,
 629 the temporal change in DIC_{cf} differs between cores, consistent with a varying role of photosynthesis
 630 (and thus metabolic carbon) among (and even within) colonies. The combined impact on cf saturation
 631 state was profound, with a significant decline of ~ 2.3 units between the 18th century and late-
 632 20th century corals ($Z = 24.2$, $N_{\text{fossil}} = 108$, $N_{\text{modern}} = 277$, $p < 0.001$). These results emphasize the
 633 importance of extending the existing boron reconstructions across time periods that experienced dif-
 634 ferent seawater chemistry from today. This initial study focused on replicate cores from one colony,
 635 and it will be critical to further replicate and extend these analyses to other fossil colonies to confirm
 636 these findings (given the potential for within and among colony differences in boron geochemistry, e.g.,
 637 Chalk et al., 2021). Nevertheless, the first such application of boron systematics to pre-industrial fos-
 638 sil coral samples, presented here, paints a potentially stark future under projected acidification, sug-
 639 gesting limited adaptive capacity in the upregulation of the coral calcifying fluid.

640 Despite this reduction in pH_{cf} between the 18th and 20th century Galápagos corals, there was
 641 no significant change in calcification or skeletal density among cores (or between modern and fossil
 642 colonies; see section "Coral densitometry and calcification" for description of methods). This is in con-
 643 trast to previous work that demonstrates a strong relationship between calcification and pH_{cf} (Ross
 644 et al., 2019; Guillermic et al., 2020), and suggests that the impact of warming on calcification kine-
 645 tics may at least partially compensate for the lower saturation (albeit with the added risk of thermal
 646 stress and bleaching). Rather, we find large interannual changes in calcification rate within (15-27%)
 647 and among (24-27%) cores (Table S6; Fig S7). The predicted change in calcification between the 18th
 648 and 20th centuries (of -10%), using predicted Ω_{sw} from Fig. 1c, the Ω_{cf} Pchange from Table S4 and
 649 the model of M. McCulloch et al. (2012), therefore falls within the range of interannual calcification
 650 variability at this site. Thus, despite large declines in Ω_{cf} , the impact on coral calcification is not yet
 651 detectable at Wolf Island, Galápagos given the high interannual calcification variability.

652 However, these results should not be interpreted as evidence that Galápagos corals are robust
 653 to changing ocean chemistry, for five reasons. First, monthly skeletal density data is strongly related
 654 to both CF saturation state and temperature in both fossil and modern Galápagos corals (Fig. 4).
 655 Although the nature of these relationships vary across cores (see Table S7; e.g., as a function of colony-
 656 to-colony variations in bleaching susceptibility), the relationships indicate declining density with warm-
 657 ing and lower cf saturation (except in core WLF-3) and an increasing importance of warming in re-
 658 cent decades (becoming the dominant predictor in core WLF-10a, ending in 2010). Second, the corals
 659 studied here are likely to represent the “best-case-scenario”, as these long-lived corals targeted for pa-
 660 leoclimate reconstructions are the “winners” that were able to maintain rapid upward extension and
 661 calcification despite thermal stress (1997/98) and acidification (Fig. S7). In smaller *P. lobata* colonies
 662 at nearby Darwin Island (D. P. Manzello et al., 2014), calcification rates were less than half those mea-
 663 sured in our longer Wolf cores, despite similar density values among colonies from both sites (Table
 664 S6). Further, the modern Wolf colonies regrew in 3.4 (WLF10-10) and 5 (WLF10-03) years follow-

665 ing the very strong 1982/83 El Niño event that devastated reefs across the Galápagos (P. W. Glynn
 666 et al., 1988), suggesting they experienced only partial mortality during this extreme event. Both colonies
 667 also displayed only modest reductions in extension and calcification during or following the 1997/98
 668 event (Figure S7). Because paleoclimate records are biased towards corals that survive, they likely
 669 yield a conservative (i.e., too-stable) estimates of past calcification changes. Third, observed and sim-
 670 ulated ocean pH at Galápagos remained above 8.0 over this period (mean CESM1 = 8.08-8.11 over
 671 intervals of coral coverage; Darwin = 8.07, Humphreys et al., 2018), a critical tipping point below which
 672 corals across the archipelago suffer reduced calcification and structural persistence (D. P. Manzello
 673 et al., 2014). High nutrients (D. P. Manzello et al., 2014) and variable seawater conditions exacerbate
 674 the stressful impacts of acidification in upwelling regions, resulting in tipping points at higher pH val-
 675 ues (D. P. Manzello et al., 2014). Fourth, the temperature dependence of calcification kinetics does
 676 not appear to compensate for the impacts of saturation-state changes at Wolf (unlike in more opti-
 677 mal environments; Burton & Walter, 1987; J. Lough & Barnes, 2000). Lastly, and critically, we demon-
 678 strate that as oceans acidify, Wolf corals have not intensified their upregulation of pH or Ω , suggest-
 679 ing that continued OA is likely to have significant impacts on calcification at this site.

680 Finally, our results support the potential to reconstruct changes in paleo-pH from the geochem-
 681 istry of coral calcifying fluid. Consistent with recent studies (Guo, 2019; J. P. D’Olivo et al., 2019),
 682 the narrow range in pH_{cf} upregulation of *Porites* spp. across sites and time periods (Table S4) sug-
 683 gests that within this paleo-relevant genus, long-term pH_{cf} trends are primarily driven by pH_{sw} and
 684 not physiological controls (which regulate calcifying fluid chemistry on seasonal timescales, in response
 685 to temperature-related changes in DIC, calcification, and buffering capacity). Physiological limits in
 686 this capacity to regulate pH_{cf} —identified here for the first time—suggest that as seawater saturation
 687 shifts to lower values (as observed with ocean acidification, or across spatial gradients, D. P. Manzello
 688 et al., 2014), so will the distribution of carbonate saturation in the calcifying fluid (as observed be-
 689 tween 18th and 20th corals). Corals’ capacity to buffer against ocean acidification may therefore be
 690 more limited than predicted from experimental manipulations and extreme environments (CO_2 seeps),
 691 with particularly severe consequences for corals at marginal sites characterized by reduced metabolic
 692 carbon production, low seawater pH, and frequent or severe stress.

693 Summary

694 In presenting the first analysis of calcifying fluid geochemistry in pre-industrial and modern corals
 695 from a marginal environment, we are able to reconcile two seemingly competing truths about the ca-
 696 pacity for corals to buffer against changing environmental conditions. On the one hand, we provide
 697 further evidence that corals are able to strongly upregulate the pH of their internal growth medium
 698 to maintain supersaturation in response to seasonal changes in DIC and temperature. This physiologically-
 699 driven seasonal upregulation of pH_{cf} precludes the use of boron isotope geochemistry for reconstruct-
 700 ing short-term variations in paleo- pH_{sw} , but suggests that corals may be able to buffer against chang-
 701 ing ocean conditions and maintain calcification under future warming and OA. On the other hand,
 702 recent work suggests that long-term trends in pH_{cf} inferred from boron isotope geochemistry are driven
 703 primarily by pH_{sw} (J. P. D’Olivo et al., 2019), suggesting at least some sensitivity to environmental
 704 conditions. However, the resource-intensive nature of boron isotope geochemistry has limited the pro-
 705 duction of long reconstructions with which to assess corals’ buffering capacity under changing ocean
 706 conditions and therefore corals’ resilience to future warming and acidification.

707 Using cores from a pre-industrial fossil and two modern coral colonies from the Galápagos Islands—
 708 a marginal environment characterized by high environmental variability, low seawater pH, and fre-
 709 quent thermal stress—we identify significant declines in pH_{cf} and Ω_{cf} with warming and OA since the
 710 pre-industrial period. These trends are exacerbated during and after thermal stress events observed

711 in the modern corals, likely due to the impact of bleaching on metabolic DIC production and the energy-
712 intensive active transport that concentrates alkalinity against the electrochemical gradients. Critically,
713 we demonstrate that these changes may be attributed to a remarkably narrow range of pH_{cf} upreg-
714 ulation across sites and time periods, suggesting a strict physiological limit in corals' ability to reg-
715 ulate their internal carbonate chemistry. We therefore find that the capacity of corals to maintain stable
716 Ω_{cf} supersaturation is dictated (to the first order) by their capacity to upregulate DIC_{cf} via metabolic
717 processes, which is reduced both at marginal sites and following bleaching. Such physiological lim-
718 its in this capacity to regulate pH_{cf} —identified here for the first time—suggest that corals' capacity
719 to buffer against ocean acidification may be more limited than predicted from experimental manip-
720 ulations and extreme environments (e.g., CO_2 seeps). These findings have particularly severe conse-
721 quences for coral calcification and thus reef structure and function at marginal sites.

722 **Acknowledgments**

723 We thank the Charles Darwin Station and the Parque Nacional Galápagos, particularly Galo Quezada,
724 for field work support and permitting for coral collection. We also thank Colin Chilcott, Meriwether
725 Wilson, Roberto Pepolas, Diego Ruiz, Jenifer Suarez, and the captain and crew of the Queen Mabel
726 for their assistance in the field. This work is supported by National Science Foundation grants 1401326/1829613
727 and 0957881 to J.E.C.; UK Natural Environment Research Council grant NE/H009957/1 to A.T.; Uni-
728 versity of Arizona Honors College Alumni Legacy Grant to A.H.C.; ARC Centre of Excellence grant
729 CE140100020 to MM and J.P.D.; and startup funds awarded to D.T. from Boston University. AIMS
730 is a federally funded government research agency. This publication is contribution number 2434 of the
731 Charles Darwin Foundation for the Galapagos Islands

732 **Competing Interests**

733 The authors declare that they have no competing financial interests.

734 **Data Availability**

735 All geochemical data will be publicly available on the National Center for Environmental Infor-
736 mation (formerly the National Climatic Data Center) paleoclimatology database (on or before pub-
737 lication).

738 **Correspondence**

739 Correspondence and requests for materials should be addressed to D.M.T. (email: thompod@arizona.edu).

740 **Author contributions**

741 J.E.C. & A.T. conceived of and funded the large coral paleoclimate effort in the Galápagos Archipelago,
742 which motivated this work, and D.M.T., J.E.C. and M.M. conceived of this experiment. D.M.T., J.E.C.,
743 and A.T. collected the coral cores utilized in this study; D.M.T. prepared coral powders for paired
744 boron–trace elemental analyses, including column chemistry; D.M.T., J.P.D. and K.D. conducted the
745 geochemical analysis; D.M.T., E.V.R., A.H.C., and L.V. analyzed and compiled the longer GW10-10
746 modern and GW10-4 fossil records used here for comparison; D.M.T. and M.L. extracted, analyzed,
747 and interpreted the CESM model output; D.M.T., E.V.R., J.L. and N.C collected the X-ray density
748 measurements; D.M.T. analyzed and interpreted the data, and wrote the manuscript; and all authors
749 provided input and contributed to finalizing and revising the manuscript.

References

750

- 751 Allison, N. (2017). Reconstructing coral calcification fluid dissolved inorganic carbon chemistry
 752 from skeletal boron: An exploration of potential controls on coral aragonite B/Ca. *Heliyon*,
 753 3(8), e00387.
- 754 Allison, N., Cohen, I., Finch, A. A., Erez, J., & Tudhope, A. W. (2014). Corals concentrate dis-
 755 solved inorganic carbon to facilitate calcification. *Nature Communications*, 5(1), 1–6.
- 756 Anderson, K. D., Cantin, N. E., Heron, S. F., Pisapia, C., & Pratchett, M. S. (2017). Variation
 757 in growth rates of branching corals along Australia’s Great Barrier Reef. *Scientific reports*,
 758 7(1), 1–13.
- 759 Beck, J. W., Edwards, R. L., Ito, E., Taylor, F. W., Recy, J., Rougerie, F., . . . Henin, C. (1992).
 760 Sea-surface temperature from coral skeletal strontium/calcium ratios. *Science*, 257(5070),
 761 644–647.
- 762 Burton, E. A., & Walter, L. M. (1987). Relative precipitation rates of aragonite and Mg calcite
 763 from seawater: Temperature or carbonate ion control? *Geology*, 15(2), 111–114.
- 764 Carton, J. A., & Giese, B. S. (2008). A reanalysis of ocean climate using Simple Ocean Data As-
 765 similation (SODA). *Monthly weather review*, 136(8), 2999–3017.
- 766 Chalk, T., Standish, C., D’Angelo, C., Castillo, K., Milton, J., & Foster, G. (2021). Mapping
 767 coral calcification strategies from in situ boron isotope and trace element measurements of
 768 the tropical coral *Siderastrea siderea*. *Scientific reports*, 11.
- 769 Cheng, H., Edwards, R. L., Shen, C.-C., Polyak, V. J., Asmerom, Y., Woodhead, J., . . . others
 770 (2013). Improvements in ²³⁰Th dating, ²³⁰Th and ²³⁴U half-life values, and U–Th isotopic
 771 measurements by multi-collector inductively coupled plasma mass spectrometry. *Earth and*
 772 *Planetary Science Letters*, 371, 82–91.
- 773 Cheung, A. H., Cole, J. E., Thompson, D. M., Vetter, L., Jimenez, G., & Tudhope, A. W. (2021).
 774 Fidelity of the coral Sr/Ca paleothermometer following heat stress in the northern Galápa-
 775 gos. *Paleoceanography and Paleoclimatology*, e2021PA004323.
- 776 Clarke, H., D’Olivo, J., Conde, M., Evans, R., & McCulloch, M. (2019). Coral Records of Vari-
 777 able Stress Impacts and Possible Acclimatization to Recent Marine Heat Wave Events on
 778 the Northwest Shelf of Australia. *Paleoceanography and Paleoclimatology*, 34(11), 1672–
 779 1688.
- 780 Clarke, H., D’Olivo, J. P., Falter, J., Zinke, J., Lowe, R., & McCulloch, M. (2017). Differential re-
 781 sponse of corals to regional mass-warming events as evident from skeletal Sr/Ca and Mg/Ca
 782 ratios. *Geochemistry, Geophysics, Geosystems*, 18(5), 1794–1809.
- 783 Corrège, T., Delcroix, T., Récy, J., Beck, W., Cabioch, G., & Le Cornec, F. (2000). Evidence for
 784 stronger El Niño-Southern Oscillation (ENSO) events in a mid-Holocene massive coral. *Pa-
 785 leoceanography*, 15(4), 465–470.
- 786 Cortés, J. (1997). Biology and geology of eastern pacific coral reefs. *Coral Reefs*, 16(1), S39–S46.
- 787 Cuny-Guirriec, K., Douville, E., Reynaud, S., Allemand, D., Bordier, L., Canesi, M., . . . oth-
 788 ers (2019). Coral Li/Mg thermometry: caveats and constraints. *Chemical Geology*, 523,
 789 162–178.
- 790 Darwin, C., & Bonney, T. G. (1889). *The structure and distribution of coral reefs*. Smith, Elder.
- 791 DeCarlo, T. M., Gaetani, G. A., Holcomb, M., & Cohen, A. L. (2015). Experimental determi-
 792 nation of factors controlling U/Ca of aragonite precipitated from seawater: Implications for
 793 interpreting coral skeleton. *Geochimica et Cosmochimica Acta*, 162, 151–165.
- 794 DeCarlo, T. M., Holcomb, M., & McCulloch, M. T. (2018). Reviews and syntheses: Revisiting the
 795 boron systematics of aragonite and their application to coral calcification. *Biogeosciences*,
 796 15(9), 2819–2834.
- 797 Dickson, A., & Millero, F. J. (1987). A comparison of the equilibrium constants for the dissocia-
 798 tion of carbonic acid in seawater media. *Deep Sea Research Part A. Oceanographic Research*

- 799 *Papers*, 34(10), 1733–1743.
- 800 Dickson, A. G. (1990). Thermodynamics of the dissociation of boric acid in synthetic seawater
801 from 273.15 to 318.15 K. *Deep Sea Research Part A. Oceanographic Research Papers*, 37(5),
802 755–766.
- 803 Dishon, G., Fisch, J., Horn, I., Kaczmarek, K., Bijma, J., Gruber, D. F., . . . Tchernov, D. (2015).
804 A novel paleo-bleaching proxy using boron isotopes and high-resolution laser ablation to
805 reconstruct coral bleaching events. *Biogeosciences*, 12(19), 5677–5687.
- 806 D’Olivo, J., & McCulloch, M. (2017). Response of coral calcification and calcifying fluid composi-
807 tion to thermally induced bleaching stress. *Scientific reports*, 7(1), 1–15.
- 808 D’Olivo, J. P., Ellwood, G., DeCarlo, T. M., & McCulloch, M. T. (2019). Deconvolving the
809 long-term impacts of ocean acidification and warming on coral biomineralisation. *Earth and*
810 *Planetary Science Letters*, 526, 115785.
- 811 D’Olivo, J. P., Sinclair, D. J., Rankenburg, K., & McCulloch, M. T. (2018). A universal multi-
812 trace element calibration for reconstructing sea surface temperatures from long-lived Porites
813 corals: Removing ‘vital-effects’. *Geochimica et Cosmochimica Acta*, 239, 109–135.
- 814 Edwards, R. L., Chen, J., & Wasserburg, G. (1987). 238U-234U-230Th-232Th systematics and
815 the precise measurement of time over the past 500,000 years. *Earth and Planetary Science*
816 *Letters*, 81(2-3), 175–192.
- 817 Foster, G., Pogge von Strandmann, P. A., & Rae, J. (2010). Boron and magnesium isotopic com-
818 position of seawater. *Geochemistry, Geophysics, Geosystems*, 11(8).
- 819 Gagnon, A. C., Gothmann, A. M., Branson, O., Rae, J. W., & Stewart, J. A. (2021). Controls on
820 boron isotopes in a cold-water coral and the cost of resilience to ocean acidification. *Earth*
821 *and Planetary Science Letters*, 554, 116662.
- 822 Gattuso, J.-P., Kirkwood, W., Barry, J., Cox, E., Gazeau, F., Hansson, L., . . . others (2014).
823 Free-ocean CO₂ enrichment (FOCE) systems: present status and future developments.
824 *Biogeosciences (BG)*, 11(15), 4057–4075.
- 825 Georgiou, L., Falter, J., Trotter, J., Kline, D. I., Holcomb, M., Dove, S. G., . . . McCulloch, M.
826 (2015). pH homeostasis during coral calcification in a free ocean CO₂ enrichment (FOCE)
827 experiment, Heron Island reef flat, Great Barrier Reef. *Proceedings of the National Academy*
828 *of Sciences*, 112(43), 13219–13224.
- 829 Glynn, P. (2001). Eastern Pacific coral reef ecosystems. In *Coastal marine ecosystems of latin*
830 *america* (pp. 281–305). Springer.
- 831 Glynn, P. W., Alvarado, J. J., Banks, S., Cortés, J., Feingold, J. S., Jiménez, C., . . . others
832 (2017). Eastern pacific coral reef provinces, coral community structure and composition: an
833 overview. In *Coral reefs of the eastern tropical Pacific* (pp. 107–176). Springer.
- 834 Glynn, P. W., Cortés-Núñez, J., Guzmán-Espinal, H. M., & Richmond, R. H. (1988). El Niño
835 (1982-83) associated coral mortality and relationship to sea surface temperature devia-
836 tions in the tropical eastern Pacific. Mortalidad de corales asociada con El Niño (1982-83)
837 y relación con las desviaciones de la temperatura superficial del mar en el Pacífico oriental
838 tropical. In *Proceedings of the 6th international coral reef symposium, australia*. (Vol. 3, pp.
839 237–243).
- 840 Glynn, P. W., Feingold, J. S., Baker, A., Banks, S., Baums, I. B., Cole, J., . . . others (2018).
841 State of corals and coral reefs of the Galápagos Islands (Ecuador): Past, present and future.
842 *Marine pollution bulletin*, 133, 717–733.
- 843 Guillermic, M., Cameron, L. P., De Corte, I., Misra, S., Bijma, J., de Beer, D., . . . Eagle, R. A.
844 (2020). Thermal stress reduces pocilloporid coral resilience to ocean acidification by impair-
845 ing control over calcifying fluid chemistry. *Science Advances*, 7(2), eaba9958.
- 846 Guo, W. (2019). Seawater temperature and buffering capacity modulate coral calcifying pH. *Sci-*
847 *entific reports*, 9(1), 1–13.

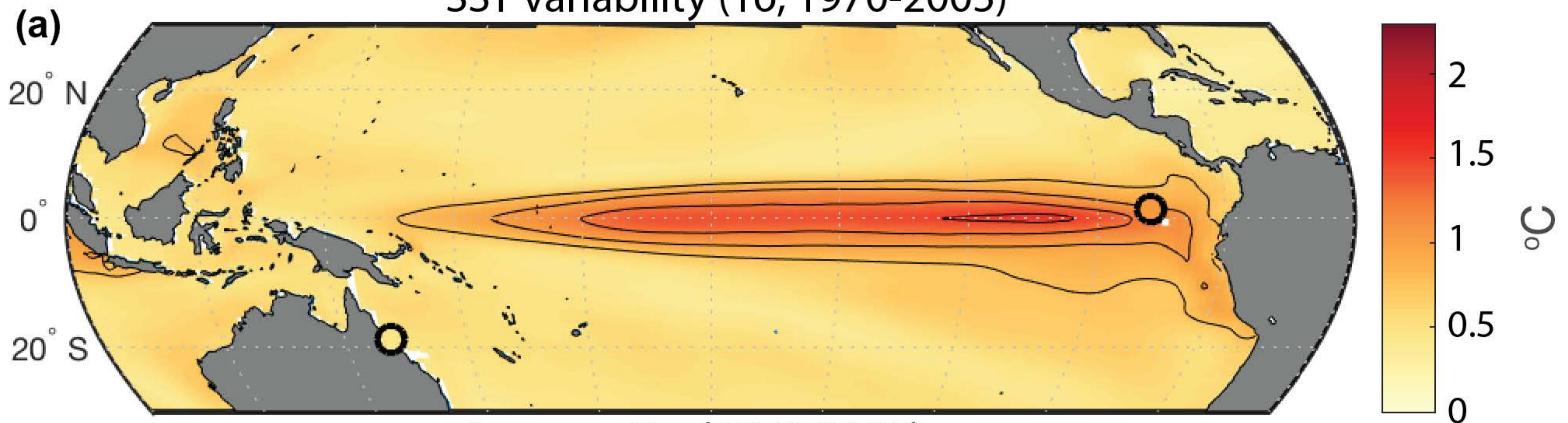
- 848 Gutjahr, M., Bordier, L., Douville, E., Farmer, J., Foster, G. L., Hathorne, E. C., ... others
 849 (2021). Sub-permil interlaboratory consistency for solution-based boron isotope analyses on
 850 marine carbonates. *Geostandards and Geoanalytical Research*, 45(1), 59–75.
- 851 Hathorne, E. C., Felis, T., Suzuki, A., Kawahata, H., & Cabioch, G. (2013). Lithium in the
 852 aragonite skeletons of massive Porites corals: A new tool to reconstruct tropical sea surface
 853 temperatures. *Paleoceanography*, 28(1), 143–152.
- 854 Hathorne, E. C., Gagnon, A., Felis, T., Adkins, J., Asami, R., Boer, W., ... others (2013). Inter-
 855 laboratory study for coral Sr/Ca and other element/Ca ratio measurements. *Geochemistry,
 856 Geophysics, Geosystems*, 14(9), 3730–3750.
- 857 Hemming, N., Guilderson, T., & Fairbanks, R. (1998). Seasonal variations in the boron isotopic
 858 composition of coral: A productivity signal? *Global biogeochemical cycles*, 12(4), 581–586.
- 859 Holcomb, M., DeCarlo, T., Gaetani, G., & McCulloch, M. (2016). Factors affecting B/Ca ratios
 860 in synthetic aragonite. *Chemical Geology*, 437, 67–76.
- 861 Holcomb, M., DeCarlo, T., Schoepf, V., Dissard, D., Tanaka, K., & McCulloch, M. (2015). Clean-
 862 ing and pre-treatment procedures for biogenic and synthetic calcium carbonate powders
 863 for determination of elemental and boron isotopic compositions. *Chemical Geology*, 398,
 864 11–21.
- 865 Humphreys, A. F., Halfar, J., Ingle, J. C., Manzello, D., Reymond, C. E., Westphal, H., & Riegl,
 866 B. (2018). Effect of seawater temperature, pH, and nutrients on the distribution and char-
 867 acter of low abundance shallow water benthic foraminifera in the Galápagos. *PLoS one*,
 868 13(9).
- 869 Hurrell, J. W., Holland, M. M., Gent, P. R., Ghan, S., Kay, J. E., Kushner, P., ... others (2013).
 870 The community earth system model: a framework for collaborative research. *Bulletin of the
 871 American Meteorological Society*, 94(9), 1339–1360.
- 872 Jimenez, G., Cole, J. E., Thompson, D. M., & Tudhope, A. W. (2018). Northern Galápagos
 873 corals reveal twentieth century warming in the eastern tropical Pacific. *Geophysical Re-
 874 search Letters*, 45(4), 1981–1988.
- 875 Kay, J. E., Deser, C., Phillips, A., Mai, A., Hannay, C., Strand, G., ... others (2015). The
 876 Community Earth System Model (CESM) large ensemble project: A community resource
 877 for studying climate change in the presence of internal climate variability. *Bulletin of the
 878 American Meteorological Society*, 96(8), 1333–1349.
- 879 Keeling, C. D. (1979). The Suess effect: ¹³Carbon-¹⁴Carbon interrelations. *Environment Interna-
 880 tional*, 2(4-6), 229–300.
- 881 Kessler, W. S. (2006). The circulation of the eastern tropical Pacific: A review. *Progress in
 882 Oceanography*, 69(2-4), 181–217.
- 883 Klochko, K., Kaufman, A. J., Yao, W., Byrne, R. H., & Tossell, J. A. (2006). Experimental mea-
 884 surement of boron isotope fractionation in seawater. *Earth and Planetary Science Letters*,
 885 248(1-2), 276–285.
- 886 Knebel, O., Carvajal, C., Standish, C. D., Vega, E. d. l., Chalk, T. B., Ryan, E. J., ... Kench, P.
 887 (2021). Porites Calcifying Fluid pH on Seasonal to Diurnal Scales. *Journal of Geophysical
 888 Research: Oceans*, 126(3), e2020JC016889.
- 889 Lauvset, S. K., Key, R. M., Olsen, A., van Heuven, S., Velo, A., Lin, X., ... others (2016). A new
 890 global interior ocean mapped climatology: The 1 × 1 GLODAP version 2. *Earth System Sci-
 891 ence Data*, 8, 325–340.
- 892 Lea, D. W., Shen, G. T., & Boyle, E. A. (1989). Coralline barium records temporal variability in
 893 equatorial Pacific upwelling. *Nature*, 340(6232), 373–376.
- 894 Lewis, E., Wallace, D., & Allison, L. J. (1998). *Program developed for CO₂ system cal-
 895 culations* (Tech. Rep.). Brookhaven National Lab., Dept. of Applied Science, Upton, NY
 896 (United States ...)

- 897 Lough, J., & Barnes, D. (2000). Environmental controls on growth of the massive coral *Porites*.
 898 *Journal of experimental marine biology and ecology*, *245*(2), 225–243.
- 899 Lough, J. M. (2010). Climate records from corals. *Wiley interdisciplinary reviews: climate*
 900 *change*, *1*(3), 318–331.
- 901 Manzello, D. (2009). Reef development and resilience to acute (El Nino warming) and chronic
 902 (high-CO₂) disturbances in the eastern tropical Pacific: a real-world climate change model.
 903 In *Proc 11th int coral reef symp* (Vol. 1, pp. 1299–1304).
- 904 Manzello, D. P. (2010). Ocean acidification hotspots: Spatiotemporal dynamics of the seawater
 905 CO₂ system of eastern Pacific coral reefs. *Limnology and Oceanography*, *55*(1), 239–248.
- 906 Manzello, D. P., Enochs, I. C., Bruckner, A., Renaud, P. G., Kolodziej, G., Budd, D. A., ...
 907 Glynn, P. W. (2014). Galápagos coral reef persistence after ENSO warming across an
 908 acidification gradient. *Geophysical Research Letters*, *41*(24), 9001–9008.
- 909 Manzello, D. P., Kleypas, J. A., Budd, D. A., Eakin, C. M., Glynn, P. W., & Langdon, C. (2008).
 910 Poorly cemented coral reefs of the eastern tropical Pacific: Possible insights into reef devel-
 911 opment in a high-CO₂ world. *Proceedings of the National Academy of Sciences*, *105*(30),
 912 10450–10455.
- 913 Mavromatis, V., Montouillout, V., Noireaux, J., Gaillardet, J., & Schott, J. (2015). Characteri-
 914 zation of boron incorporation and speciation in calcite and aragonite from co-precipitation
 915 experiments under controlled pH, temperature and precipitation rate. *Geochimica et Cos-
 916 mochimica Acta*, *150*, 299–313.
- 917 McConnaughey, T. (1989). ¹³C and ¹⁸O isotopic disequilibrium in biological carbonates: II.
 918 In vitro simulation of kinetic isotope effects. *Geochimica et Cosmochimica Acta*, *53*(1), 163–
 919 171.
- 920 McCulloch, M., Falter, J., Trotter, J., & Montagna, P. (2012). Coral resilience to ocean acidifica-
 921 tion and global warming through pH up-regulation. *Nature Climate Change*, *2*(8), 623–627.
- 922 McCulloch, M. T., D’Olivo, J. P., Falter, J., Holcomb, M., & Trotter, J. A. (2017). Coral calci-
 923 fication in a changing world and the interactive dynamics of pH and DIC upregulation. *Na-
 924 ture communications*, *8*(1), 1–8.
- 925 McCulloch, M. T., Holcomb, M., Rankenburg, K., & Trotter, J. A. (2014). Rapid, high-precision
 926 measurements of boron isotopic compositions in marine carbonates. *Rapid Communications
 927 in Mass Spectrometry*, *28*(24), 2704–2712.
- 928 Mehrbach, C., Culberson, C., Hawley, J., & Pytkowicz, R. (1973). Measurement of the appar-
 929 ent dissociation constants of carbonic acid in seawater at atmospheric pressure 1. *Limnology
 930 and Oceanography*, *18*(6), 897–907.
- 931 Montagna, P., McCulloch, M., Douville, E., Correa, M. L., Trotter, J., Rodolfo-Metalpa, R., ...
 932 others (2014). Li/Mg systematics in scleractinian corals: Calibration of the thermometer.
 933 *Geochimica et Cosmochimica Acta*, *132*, 288–310.
- 934 Mucci, A. (1983). The solubility of calcite and aragonite in seawater at various salinities, temper-
 935 atures, and one atmosphere total pressure. *American Journal of Science*, *283*(7), 780–799.
- 936 Noireaux, J., Mavromatis, V., Gaillardet, J., Schott, J., Montouillout, V., Louvat, P., ...
 937 Neuville, D. (2015). Crystallographic control on the boron isotope paleo-pH proxy. *Earth
 938 and Planetary Science Letters*, *430*, 398–407.
- 939 Otto-Bliesner, B. L., Brady, E. C., Fasullo, J., Jahn, A., Landrum, L., Stevenson, S., ... Strand,
 940 G. (2016). Climate variability and change since 850 CE: An ensemble approach with the
 941 Community Earth System Model. *Bulletin of the American Meteorological Society*, *97*(5),
 942 735–754.
- 943 Pelejero, C., Calvo, E., McCulloch, M. T., Marshall, J. F., Gagan, M. K., Lough, J. M., &
 944 Opdyke, B. N. (2005). Preindustrial to modern interdecadal variability in coral reef pH.
 945 *Science*, *309*(5744), 2204–2207.

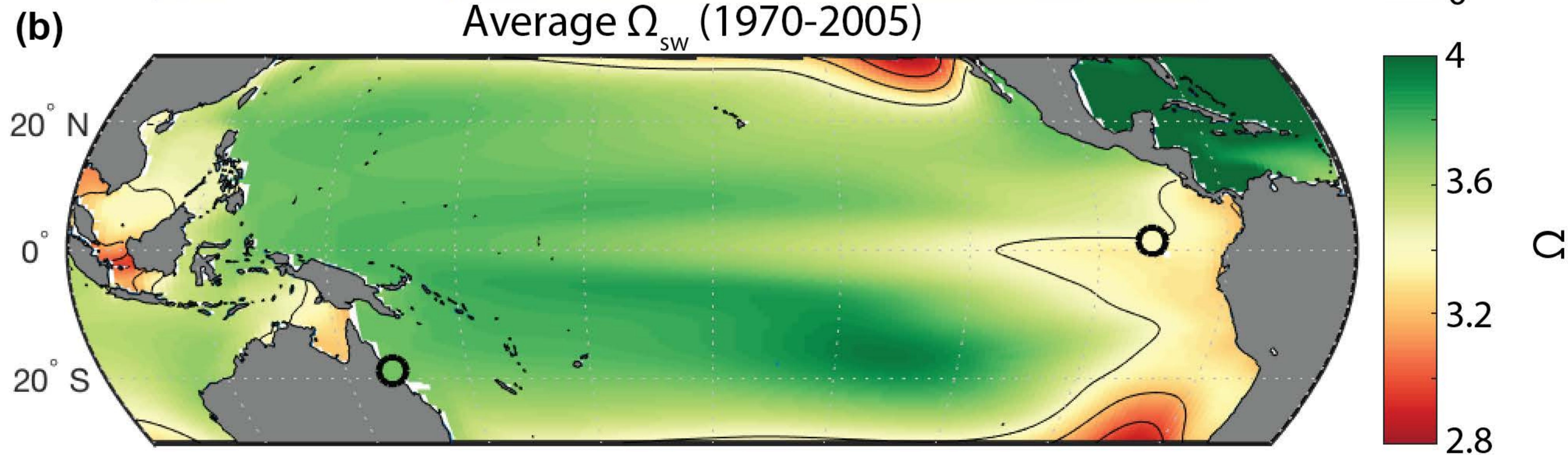
- 946 Reed, E. V., Cole, J. E., Lough, J. M., Thompson, D., & Cantin, N. E. (2019). Linking climate
947 variability and growth in coral skeletal records from the Great Barrier Reef. *Coral Reefs*,
948 *38*(1), 29–43.
- 949 Reed, E. V., Thompson, D. M., Cole, J. E., Lough, J. M., Cantin, N. E., Cheung, A. H., ... Ed-
950 wards, R. L. (2021). Impacts of coral growth on geochemistry: Lessons from the galápagos
951 islands. *Paleoceanography and Paleoclimatology*, *36*(4), e2020PA004051.
- 952 Reynolds, R. W., Rayner, N. A., Smith, T. M., Stokes, D. C., & Wang, W. (2002). An improved
953 in situ and satellite SST analysis for climate. *Journal of climate*, *15*(13), 1609–1625.
- 954 Reynolds, R. W., Smith, T. M., Liu, C., Chelton, D. B., Casey, K. S., & Schlax, M. G. (2007).
955 Daily high-resolution-blended analyses for sea surface temperature. *Journal of Climate*,
956 *20*(22), 5473–5496.
- 957 Ross, C. L., DeCarlo, T. M., & McCulloch, M. T. (2019). Environmental and physiochemical
958 controls on coral calcification along a latitudinal temperature gradient in Western Australia.
959 *Global change biology*, *25*(2), 431–447.
- 960 Ross, C. L., Falter, J. L., & McCulloch, M. T. (2017). Active modulation of the calcifying fluid
961 carbonate chemistry ($\delta^{11}\text{B}$, B/Ca) and seasonally invariant coral calcification at sub-
962 tropical limits. *Scientific reports*, *7*(1), 1–11.
- 963 Sayani, H. R., Thompson, D. M., Carilli, J. E., Marchitto, T. M., Chapman, A. U., & Cobb,
964 K. M. (2021). Reproducibility of Coral Mn/Ca-Based Wind Reconstructions at Kir-
965 itimati Island and Butaritari Atoll. *Geochemistry, Geophysics, Geosystems*, *22*(3),
966 e2020GC009398.
- 967 Schoepf, V., D’Olivo, J. P., Rigal, C., Jung, E. M. U., & McCulloch, M. T. (2021). Heat stress
968 differentially impacts key calcification mechanisms in reef-building corals. *Coral Reefs*,
969 *40*(2), 459–471.
- 970 Schoepf, V., Grottoli, A. G., Levas, S. J., Aschaffenburg, M. D., Baumann, J. H., Matsui, Y., &
971 Warner, M. E. (2015). Annual coral bleaching and the long-term recovery capacity of coral.
972 *Proceedings of the Royal Society B: Biological Sciences*, *282*(1819), 20151887.
- 973 Sen, S., Stebbins, J., Hemming, N., & Ghosh, B. (1994). Coordination environments of B impu-
974 rities in calcite and aragonite polymorphs: a ^{11}B MAS NMR study. *American Mineralogist*,
975 *79*(9–10), 819–825.
- 976 Sevilgen, D. S., Venn, A. A., Hu, M. Y., Tambutté, E., de Beer, D., Planas-Bielsa, V., & Tam-
977 butté, S. (2019). Full in vivo characterization of carbonate chemistry at the site of calcifica-
978 tion in corals. *Science advances*, *5*(1), eaau7447.
- 979 Shen, C.-C., Edwards, R. L., Cheng, H., Dorale, J. A., Thomas, R. B., Moran, S. B., ... Ed-
980 monds, H. N. (2002). Uranium and thorium isotopic and concentration measurements by
981 magnetic sector inductively coupled plasma mass spectrometry. *Chemical Geology*, *185*(3–4),
982 165–178.
- 983 Shen, G. T., Cole, J. E., Lea, D. W., Linn, L. J., McConnaughey, T. A., & Fairbanks, R. G.
984 (1992). Surface ocean variability at galapagos from 1936–1982: calibration of geochemical
985 tracers in corals. *Paleoceanography*, *7*(5), 563–588.
- 986 Spalding, M., Burke, L., Wood, S. A., Ashpole, J., Hutchison, J., & Zu Ermgassen, P. (2017).
987 Mapping the global value and distribution of coral reef tourism. *Marine Policy*, *82*, 104–
988 113.
- 989 Sutton, A. J., Feely, R. A., Maenner-Jones, S., Musielwicz, S., Osborne, J., Dietrich, C., ... oth-
990 ers (2019). Autonomous seawater pCO₂ and pH time series from 40 surface buoys and the
991 emergence of anthropogenic trends. *Earth System Science Data*, 421.
- 992 Sutton, A. J., Feely, R. A., Sabine, C. L., McPhaden, M. J., Takahashi, T., Chavez, F. P., ...
993 Mathis, J. T. (2014). Natural variability and anthropogenic change in equatorial Pacific
994 surface ocean pCO₂ and pH. *Global Biogeochemical Cycles*, *28*(2), 131–145.

- 995 Swart, P. K. (1983). Carbon and oxygen isotope fractionation in scleractinian corals: a review.
996 *Earth-science reviews*, 19(1), 51–80.
- 997 Thompson, D. M. (2021). Environmental records from coral skeletons: A decade of novel insights
998 and innovation. *Wiley Interdisciplinary Reviews: Climate Change*, e745.
- 999 Wall, M., Fietzke, J., Crook, E., & Paytan, A. (2019). Using B isotopes and B/Ca in corals
1000 from low saturation springs to constrain calcification mechanisms. *Nature communications*,
1001 10(1), 1–9.
- 1002 Wall, M., Fietzke, J., Schmidt, G. M., Fink, A., Hofmann, L., De Beer, D., & Fabricius, K.
1003 (2016). Internal pH regulation facilitates in situ long-term acclimation of massive corals
1004 to end-of-century carbon dioxide conditions. *Scientific reports*, 6, 30688.
- 1005 Weber, J. N., & Woodhead, P. M. (1972). Temperature dependence of oxygen-18 concentration in
1006 reef coral carbonates. *Journal of Geophysical Research*, 77(3), 463–473.
- 1007 Zeebe, R. E., & Wolf-Gladrow, D. (2001). *CO₂ in seawater: equilibrium, kinetics, isotopes*
1008 (No. 65). Gulf Professional Publishing.

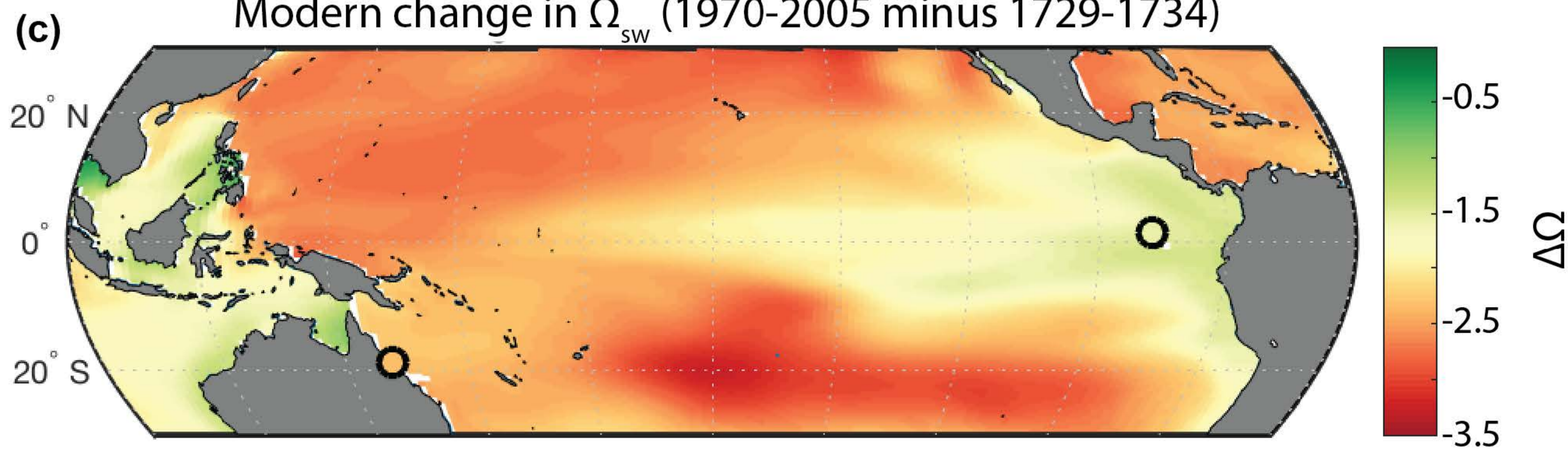
SST variability (1σ , 1970-2005)

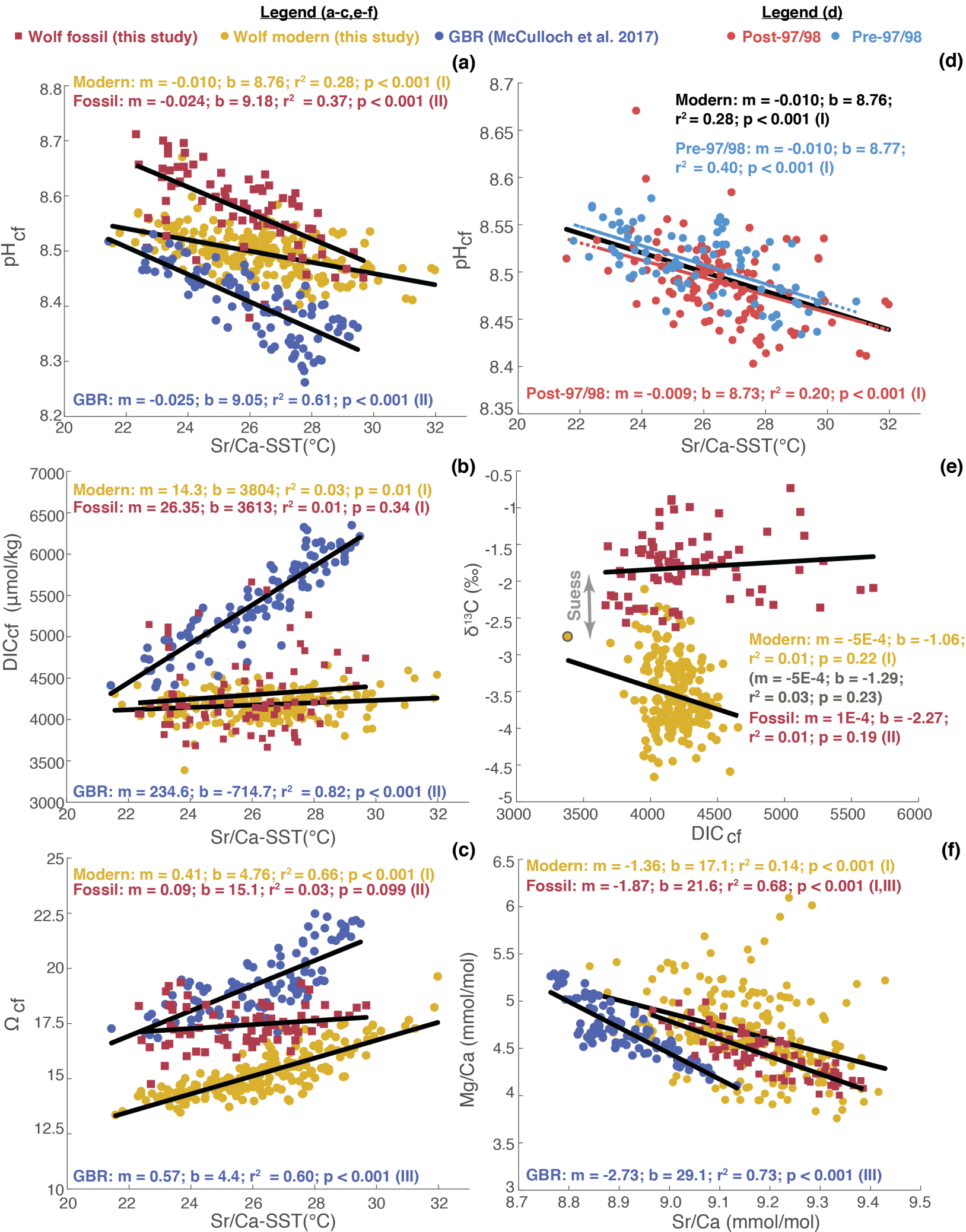


Average Ω_{sw} (1970-2005)



Modern change in Ω_{sw} (1970-2005 minus 1729-1734)





Pre-industrial

Modern

Seawater

(a) Cold season
 ↑ upwelling ↓ SST
 ↑ DIC_{sw} ↓ δ¹³C_{DIC}
 ↑ light

(b) Warm season
 ↓ upwelling ↑ SST
 ↓ DIC_{sw} ↑ δ¹³C_{DIC}
 ↓ light

↑ SST ↑ ΔSST
 ↓ Ω_{sw} ↓ δ¹³C_{DIC}

Physiological processes

↑ photosynthesis

↓ photosynthesis

(c) Cold season

**(d) Warm season
(amplified in El Niño)**

Long-term changes



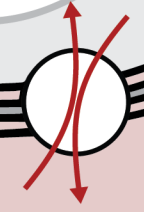
↑ photosynthesis

↓ photosynthesis

bleaching

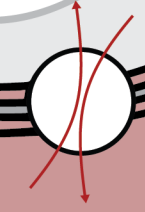
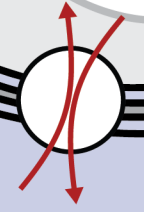
Calcifying fluid

↑ active transport



↓ active transport

↑ active transport



↓↓ active transport

↓ pH_{cf} ↓ Ω_{cf}
 ↑ ΔΩ_{cf} ↓ δ¹³C_{cf}

↑ pH_{cf} ↓ Ω_{cf} ↓ pH_{cf} ↑ Ω_{cf}
 — DIC_{cf} ↑ δ¹³C_{cf} — DIC_{cf} ↓ δ¹³C_{cf}

Skeleton

↑ Sr/Ca



↓ Sr/Ca

↑ Sr/Ca



↓ Sr/Ca

